AGU PUBLICATIONS

JGR

Journal of Geophysical Research: Oceans

RESEARCH ARTICLE

10.1002/2016JC012008

Carbon cycling dynamics in the seasonal sea-ice zone of East Antarctica

Nicholas P. Roden[1,2,3], Bronte Tilbrook[2,3], Thomas W. Trull[2,3], Patti Virtue[1,3], and Guy D. Williams[1,3]

[1]Institute for Marine and Antarctic Studies, University of Tasmania, Hobart, Tasmania, Australia, [2]CSIRO Oceans and Atmosphere, Hobart, Tasmania, Australia, [3]Antarctic Climate and Ecosystems Cooperative Research Centre, University of Tasmania, Hobart, Tasmania, Australia

Key Points:
- Large variability in the biological and physical drivers of carbon cycling dynamics was observed
- The East Antarctic seasonal ice zone was a weak net source of CO_2 to the atmosphere during the ice-free period
- Seasonally integrated estimates of net community production were as high as 6.4 mol C m^{-2}, but on average were found to be 1.3 ± 0.9 mol C m^{-2}

Supporting Information:
- Supporting Information S1
- Figure S1
- Figure S2
- Figure S3
- Figure S4
- Figure S5

Correspondence to:
N. Roden,
nick.roden@utas.edu.au

Citation:
Roden, N. P., B. Tilbrook, T. W. Trull, P. Virtue, and G. D. Williams (2016), Carbon cycling dynamics in the seasonal sea-ice zone of East Antarctica, *J. Geophys. Res. Oceans*, *121*, 8749–8769, doi:10.1002/2016JC012008.

Received 1 JUN 2016
Accepted 3 NOV 2016
Accepted article online 11 NOV 2016
Published online 19 DEC 2016

Abstract The carbon cycle of the seasonally ice covered region of the southwest Indian Ocean sector of East Antarctica (30°–80°E, 60°–69°S) was investigated during austral summer (January–March 2006). Large variability in the drivers and timing of carbon cycling dynamics were observed and indicated that the study site was a weak net source of carbon dioxide (CO_2) to the atmosphere of 0.8 ± 1.6 g C m^{-2} during the ice-free period, with narrow bands of CO_2 uptake observed near the continental margin and north of the Southern Antarctic Circumpolar Current Front. Continuous surface measurements of dissolved oxygen and the fugacity of CO_2 were combined with net community production estimates from oxygen/argon ratios to show that surface heat gain and photosynthesis were responsible for the majority of observed surface water variability. On seasonal timescales, winter sea-ice cover reduced the flux of CO_2 to the atmosphere in the study area, followed by biologically driven drawdown of CO_2 as the ice retreated in spring-summer highlighting the important role that sea-ice formation and retreat has on the biogeochemical cycling of the region.

1. Introduction

The Southern Ocean plays a critical role in the global carbon cycle, accounting for over 40% of the global ocean uptake of anthropogenic carbon dioxide (CO_2) [*Sabine et al*., 2004; *Khatiwala et al*., 2009]. This area is one of the most poorly sampled ocean regions [*Lenton et al*., 2013] with observations often localized and widely separated in both space and time, resulting in a heavy dependence on models to characterize carbon fluxes at regional scales in this area. Notable discrepancies exist between model and observational results within the seasonal ice zone (SIZ) around Antarctica. Ocean biogeochemical models, for example, indicate a weak annual sink of CO_2 for the area south of 58°S, whereas atmospheric inversions show the area to be a small source [*Lenton et al*., 2013]. These discrepancies are most likely due to sparse observations and incomplete model formulations that do not adequately resolve the large seasonal variability in processes that govern atmosphere-ocean interactions, such as temperature, wind regimes, sea-ice conditions, and biological productivity [*Takahashi et al*., 2012].

Given the important role of atmospheric CO_2 in the climate system, there is a need to accurately attribute the causes of change and develop a regional understanding of the CO_2 sink/source nature of the Southern Ocean. For example, *Arrigo et al*. [2008a] modeled CO_2 uptake in the south-western Ross Sea, which equates to 27% of their CO_2 sink estimate for the entire Southern Ocean. While this suggests the shelf regions around Antarctica may be a significant component of the Southern Ocean CO_2 uptake, the quantification of their role in carbon uptake is largely unresolved. Furthermore, future change in the Southern Ocean carbon cycle is likely to be complicated by climate-related physical and biological feedbacks associated with changes in sea-ice dynamics [*Massom et al*., 2013], increased stratification [*Smith and Nelson*, 1986], and the intensification of winds [*Thompson et al*., 2011; *Meijers*, 2014]. Recent evidence indicates the efficiency of the Southern Ocean CO_2 sink has increased in the past decade [*Landschützer et al*., 2015], after weakening in the previous decade [*Le Quéré et al*., 2007], indicating changes to large-scale ocean dynamics will not only influence future atmospheric CO_2 levels, but may also influence the rate of ocean acidification in this region [*Lenton et al*., 2009].

The majority of the Southern Ocean is characterized as a high-nutrient, low-chlorophyll (HNLC) zone, which refers to areas of the ocean with low standing stocks of phytoplankton and high macronutrient

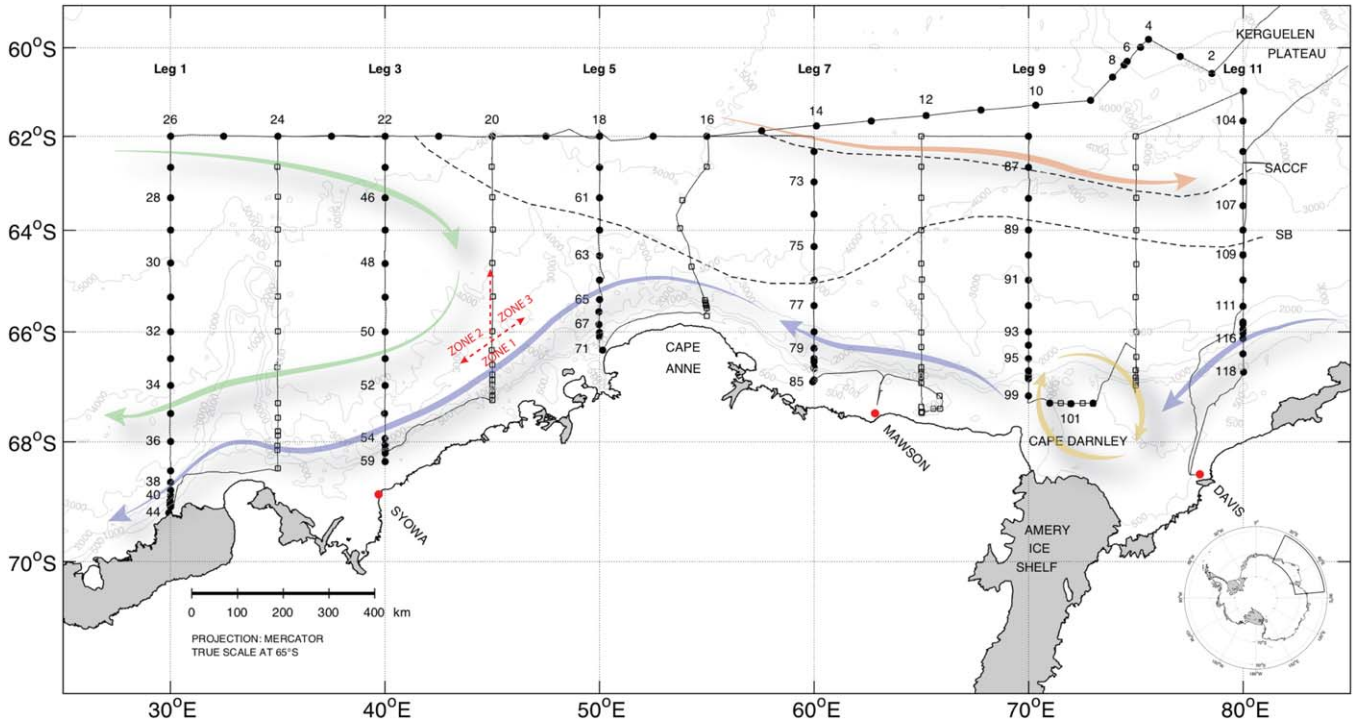

Figure 1. Cruise track of the *RV Aurora Australis* during the BROKE-West survey in the South Indian sector of the Southern Ocean. Showing the location of CTD and xCTD stations, marked as black dots and black open squares, respectively. Black-dashed lines (labeled) show the location of the Southern Boundary (SB) of Circumpolar Deep Water and the Southern Antarctic Circumpolar Current Front (SACCF). Other large-scale oceanographic features include the main flow in the east of the Weddell Gyre (green arrows), the Antarctic Slope Current (blue arrows), the Prydz Bay Gyre (yellow arrow) [*Heywood et al*., 1999], and the southern Antarctic Circumpolar Current (red arrow). The intersections of Zones 1–3 are delineated with red dashed arrows, for precise boundaries refer to text in section 2.1.1.

concentrations. Although modest rates of annual average net primary production occur in the Southern Ocean [*Arrigo et al*., 2008b], intense phytoplankton blooms can occur. The marginal ice zone (MIZ), defined as the outer edge of the summer pack ice, has been recognized as a site of elevated biomass and productivity [*Smith and Nelson*, 1986]. Here, the spring bloom of phytoplankton is initiated during the development of a stable water column formed by the input of low-density water from the receding sea-ice. Whilst sea-ice dynamics and the development of the seasonal mixed layer (SML) are undoubtedly important processes, the timing and the magnitude of primary productivity in the Southern Ocean is also driven by light availability and the supply of micronutrients, particularly iron [*de Baar et al*., 1995]. The various supply mechanisms of iron to the Southern Ocean have been widely discussed in the literature [*Sedwick and DiTullio*, 1997; *Cassar et al*., 2007; *Boyd and Mackie*, 2008; *Lannuzel et al*., 2014; *Schallenberg et al*., 2015]. Dust deposition, sea-ice melt, and the oceanic supply through sediment interactions and upwelling are considered to be among the most important processes controlling iron availability and thus, influencing the biological productivity of the Southern Ocean.

For January–March 2006, the SIZ off the coast of East Antarctica between 30° and 80°E, was the location of a comprehensive marine study. The Baseline Research on Oceanography, Krill and the Environment-West (BROKE-West) survey concentrated on the Commission for the Conservation of Antarctic Marine Living Resources (CCAMLR) statistical division 58.4.2. The statistical divisions of the CCAMLR area, which tend to align with the general ecosystem characteristics of the Southern Ocean, were implemented so that catch, effort, and trade statistics in each region could be reported. The BROKE-West survey included 11 meridional oceanographic transects over the Antarctic shelf, slope, and rise every 5° of longitude and a zonal section to the north at 62°S (Figure 1). A series of papers from the study covered the large-scale circulation [*Meijers et al*., 2010], surface oceanography [*Williams et al*., 2010], remotely sensed climatologies of the region [*Schwarz et al*., 2010], primary productivity [*Westwood et al*., 2010], phytoplankton [*Wright et al*., 2010], protistan community composition [*Davidson et al*., 2010], and krill [*Jarvis et al*., 2010; *Kawaguchi et al*., 2010; *Virtue et al*., 2010]. This paper describes the surface and vertical distribution of biogeochemical properties

Table 1. Bounding Neutral Density (γ_n), Potential Temperature (θ), and Water Depth Values That Define the Major Water Masses in the BROKE-West Region

	γ_n (kg m^{-3})	θ (°C)	Water Depth
Antarctic Surface Water (AASW)	<28.03	>−1.925	Above T_{min} base
Circumpolar Deep Water (CDW)		>1.5	Below T_{min} base to 2500 m
Modified CDW (mCDW)		≤1.5	Below T_{min} base to 2500 m
Antarctic Bottom Water (AABW)	>28.27	>−1.925	>2500
Modified Shelf Water (mSW)	>28.27	>−1.85	600–2500 m (Slope)
Low Salinity Shelf Water (LSSW)	>28.27	>−1.85	<600 m (Shelf)
Dense Shelf Water (DSW)	>28.27	−1.925 to −1.85	<600 m (Shelf)
Ice Shelf Water (ISW)		≤-1.925	

through the region, the physical and biological processes influencing the observed changes and the winter to summer evolution of such properties.

2. Data and Methods

2.1. Oceanographic Setting of the Antarctic Margin Between 30° and 80°E

2.1.1. Large-Scale Circulation and Water Mass Properties

The study region lies inside the Weddell-Enderby basin, with the Kerguelen Plateau immediately to the northeast and the Princess Elizabeth Trough to the east. The large-scale circulation, water masses, and frontal boundaries of the BROKE-West study area [*Williams et al*., 2010; *Meijers et al*., 2010], include two partial gyres, three major fronts, and six water masses and several upwelling regimes associated with the Weddell Gyre, the Antarctic Divergence, and the Kerguelen Plateau [*Foldvik and Gammelsrød*, 1988; *Park et al*., 1998; *Sokolov and Rintoul*, 2007; *Bakker et al*., 2008; *Williams et al*., 2010]. We define water masses of the region based on the classifications of *Whitworth et al*. [1998] and *Shadwick et al*. [2014] (Table 1).

The region can be divided into three distinctive zones [*Schwarz et al*., 2010] that were sampled from the surface to the bottom (Figure 1), starting with Leg 1 in January and Leg 11 completed in February. Zone 1, is the continental shelf/slope region (depth < 3000 m) to the south of the Antarctic Slope Front, and is characterized by marginal ice cover in December and January, and by the westward flowing Antarctic Slope Current. Zone 2, covers waters to the north of the Antarctic Slope Front and west of ~45°E and corresponds to the SIZ and the eastern limb of the Weddell Gyre, which is an elongated cyclonic gyre. To the east and offshore, Zone 3 contains the SIZ and includes the Prydz Bay Gyre, the Antarctic Circumpolar Current (ACC) and its southern fronts, i.e., the Southern ACC Front (SACCF) and the Southern Boundary (SB) [*Orsi et al*., 1995]. The SACCF and SB are forced southward by the Kerguelen Plateau and flow eastward through the Princess Elizabeth Trough at the eastern end of the study region.

2.1.2. Variability of Antarctic Surface Water Properties

The seasonal growth and melt of sea-ice has a significant influence on the structure and properties of surface waters in the region, as described by *Williams et al*. [2010] and summarized here. Heat loss to the atmosphere in winter drives sea-ice formation and convection, mixing the relatively cold surface waters with the warmer underlying CDW. This forms a deep, homogenous winter mixed layer with the sea-ice cap restricting sea-air gas exchange. The sea-ice begins to melt in spring-summer and melt water stratifies the surface water and warms, forming a SML. The properties of the winter mixed layer are still present at depth, recognizable by a temperature minimum, or T_{min}, layer with a seasonal pycnocline separating it from the overlying SML. South of the sea-ice edge, convection continues and a SML is absent or weak, especially over the shelf where mixing can reach the seafloor.

Sea-ice covered the BROKE-West study area during the winter prior to the survey and retreated from the north-east to the south-west from November to January (Figures 2a–2c). The sea-ice was mostly gone from the region by the start of the survey in January, apart from the westernmost legs, and persisted over the continental shelf at the southern end of most transects throughout the study. For waters north of the Antarctic Slope Front, the SML was typically about 40–60 m deep and saltier in the east and shoaled to depths as low as 12 m and freshened in the west. The deeper and saltier waters in the east appear to result from a combination of the transport of ACC waters into this eastern region and greater time since the seasonal retreat of sea-ice for wind mixing to deepen the SML [*Williams et al*., 2010].

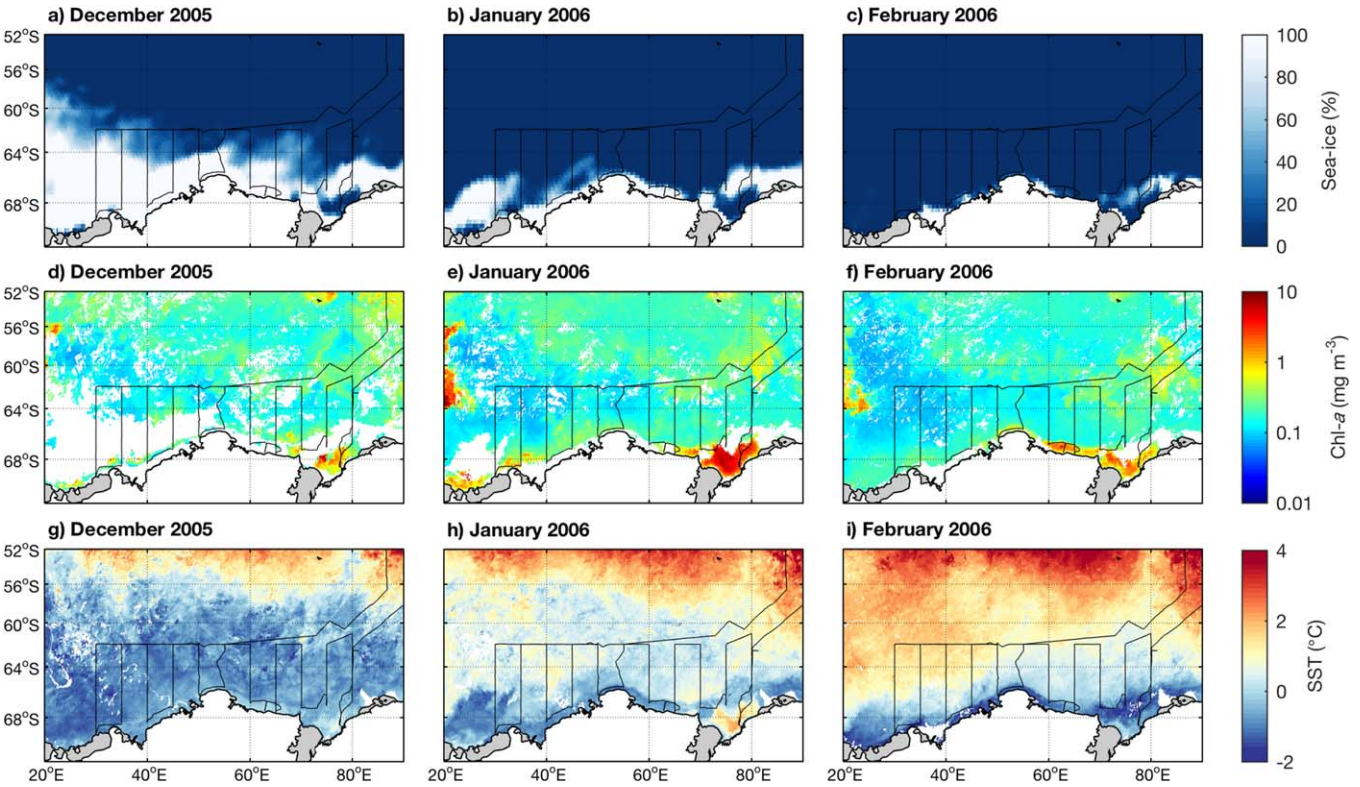

Figure 2. (a–c) Monthly satellite derived concentrations of sea-ice (%), (d–f) chlorophyll-*a* (mg m^{-3}), and (g–i) sea surface temperature (°C) with the cruise track overlaid in black. Sea-ice data are from Nimbus-7 (25 km) [*Cavalieri et al*., 2015]. Chlorophyll-*a* and sea surface temperature from MODIS-Aqua (9 km).

2.2. Biogeochemical Measurements

For a comprehensive description of oceanographic field measurements, processing and calibration from BROKE-West, see *Rosenberg and Gorton* [2006]. A total of 118 Conductivity-Temperature-Depth (CTD) casts were conducted aboard the *RV Aurora Australis* using a Sea-Bird SBE 9plus with 22 × 10 L General Oceanics Niskin bottles mounted onto a Sea-Bird rosette. Eighty expendable CTD (xCTD) probes were also used on meridional transects between the major CTD transects.

Seawater samples of 250 mL were collected from the Niskin bottles on CTD casts and were analyzed onboard for total dissolved inorganic carbon (DIC) and total alkalinity (TA). For each of these samples, 100 μL of a saturated $HgCl_2$ solution was added to halt biological activity. DIC was determined using a Single Operator Multiparameter Metabolic Analyser following the procedure in *Dickson et al*. [2007]. TA was determined by open-cell potentiometric titration using a 0.1 M hydrochloric acid titrant [*Dickson et al*., 2007]. Routine analysis of Certified Reference Material (batches 70 and 72) from Scripps Institution of Oceanography were used to verify the measurement accuracy and precision for DIC and TA analyses, which were better than ± 2 μmol kg^{-1}. Samples for dissolved phosphate (HPO_4^{2-}), silicic acid (H_4SiO_4) and nitrate + nitrite ($NO_3^- + NO_2^-$) (hereafter nitrate) were collected and analyzed spectrophotometrically [*Pasquer et al*., 2010] and yielded a measurement accuracy and precision of ± 0.05 μmol kg^{-1}, ± 1.5 μmol kg^{-1}, and ± 0.4 μmol kg^{-1}, respectively.

TA was only measured at the surface and on nine full depth CTD casts. These data were combined with data from previous cruises that used the same measurement techniques and a linear regression of salinity versus TA and nitrate (TA + N), known as potential alkalinity, was calculated. This relationship (Figure 3) was used to calculate TA at sample sites without alkalinity measurements. Data used to calculate the regression were from samples shallower than 500 m and included measurements from this study, together with those south of 60°S on CO_2/WOCE hydrographic sections of the nearby Princess Elizabeth Trough in 2005, and measurements from the southern end of the 1994 WOCE SR3 transect along 140°E. The sum of TA and nitrate concentrations accounts for changes in TA associated with

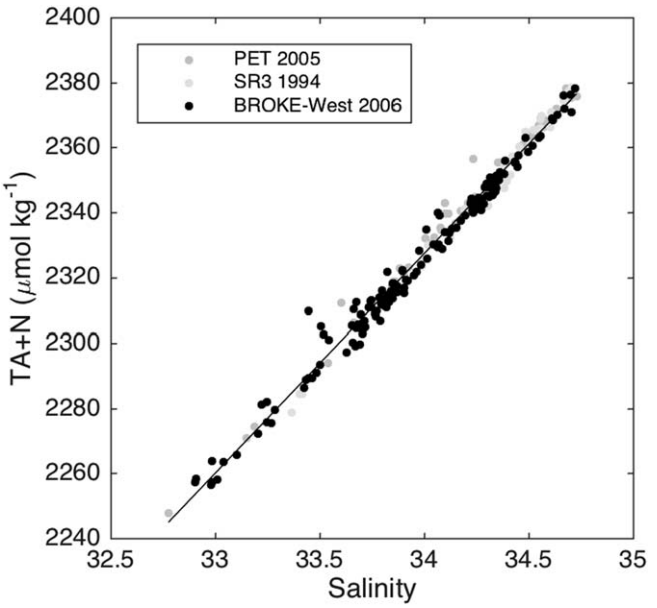

Figure 3. The salinity and TA+N relationship of waters south of 60°S and shallower than 500 m from BROKE-West in 2006, the Princess Elizabeth Trough in 2005 (PET) and from the WOCE SR3 transect, measured in 1994 (data available from GLODAP). A linear regression yielded the following equation, $y=(67\pm1)x+(36\pm18)$ ($n=237$, $r^2=0.99$, standard error = 4 μmol kg^{-1}).

the uptake or release of dissolved nitrate during photosynthesis or respiration [*Brewer and Goldman*, 1976]:

$$106\ CO_2+138\ H_2O+16\ NO_3^- \rightarrow (CH_2O)_{106}\ (NH_3)_{16}+16\ OH^-+138\ O_2 \quad (1)$$

Once TA+N values were calculated at sample sites, concurrently measured nitrate concentrations were subtracted to give an estimate of TA. The correlation between the parameters in Figure 3 ($y=(67\pm1)x+(36\pm18)$; $n=237$, $r^2=0.99$, standard error = 4 μmol kg^{-1}) indicates net calcification/dissolution of carbonate minerals in the water column was not a significant contributor to the TA variability.

High-resolution surface water measurements of the fugacity of CO_2 (fCO_2) coupled with atmospheric CO_2 measurements, were made by pumping seawater from the ship's intake into a Weiss style spray equilibrator [*Pierrot et al.*, 2009]. The accuracy and precision of the measurements is estimated to be better than ± 2 μatm (see supporting information). The sea-air gradient in fCO_2 (ΔfCO_2) was used to compute sea-air CO_2 flux using the following equation:

$$CO_{2\ flux}=k\cdot\alpha\cdot\Delta fCO_2 \quad (2)$$

where k is the gas transfer velocity (cm h^{-1}) [*Wanninkhof et al.*, 2013], scaled linearly with sea-ice cover by multiplying k by the fraction of open water, and α is the CO_2 solubility (mol m^{-3} atm^{-1}) [*Weiss*, 1974]. The gas transfer velocity was computed using measured wind speeds from the ship's 10 m wind anemometer for underway estimates of $CO_{2\ flux}$ ($CO_{2\ flux}^{uw}$). A positive sea-air $CO_{2\ flux}$ value implies a net transfer from the ocean to the atmosphere.

A calculation of the sea-air flux of CO_2 since ice retreated ($CO_{2\ flux}^{ice-free}$) was also made at each CTD station using wind speed history, sea-ice concentration, and estimates of the seasonal development of ΔfCO_2 values. The number of ice-free days at each station were estimated from the day of sampling to when sea-ice concentrations obtained from the National Snow and Ice Data Centre [*Cavalieri et al.*, 2015] first fell below 15% [*Schwarz et al.*, 2010]. The reduction from complete ice cover to 15% occurs rapidly and the time of emergence of 15% cover is considered a good marker of when surface waters become open and can exchange gas across the sea-air boundary. The wind speed history at each CTD site was taken from daily mean cross-calibrated multiplatform (CCMP) winds [*Atlas et al.*, 2011]. The sea-air gradient, ΔfCO_2, in equation (2) was estimated for each ice-free day prior to sampling at CTD sites. Atmospheric fCO_2 was calculated after *Weiss* [1974] using the mean atmospheric mole fraction of CO_2 (XCO_2) measured in the study region and sea-level pressure values from the NCEP-DOE Reanalysis 2 data product interpolated in time. Ice-free surface water fCO_2 values were estimated from linearly interpolated surface water properties from the day of sampling to the first ice-free day, assuming that surface conditions at ice-free day 0 resembled the properties observed in the T_{min} layer. It is possible that primary production may have reduced surface water fCO_2 values before ice concentrations fell below 15% [*Gibson and Trull*, 1999; *Roden et al.*, 2013] and could lead to an overestimate of the sea-air flux.

The saturation state of aragonite (Ω_{ar}) [*Mucci*, 1983], fCO_2, and pH on the seawater scale (pH_{sws}) were calculated from DIC, TA, phosphate, and silicic acid data using the standard set of carbonate system equations with the CO2SYS program [*van Heuven et al.*, 2011] and the dissociation constants of *Roy et al.* [1993]. Errors

associated with measured input parameters were incorporated into a Monte Carlo simulation to estimate uncertainties for Ω_{ar}, fCO_2 and pH_{sws} of $\pm$ 0.03, $\pm$ 14 μatm and $\pm$ 0.01, respectively [see *Roden et al*., 2013]. To estimate the concentration of anthropogenic CO_2 (C_{ant}) in the study area (Figure 9), we used the composite tracer TrOCA, which utilizes measurements of potential temperature, DIC, TA, and O_2 to estimate the anthropogenic component of DIC [*Touratier and Goyet*, 2004; *Touratier et al*., 2007]. Propagating the uncertainties associated with these measured input parameters, we estimate an uncertainty of $\pm$ 5 μmol kg^{-1} for C_{ant} estimates. The TrOCA method is not suitable for surface waters that experience large seasonal variability, which precludes estimates of C_{ant} for Antarctic Surface Water (AASW). The same method may also lead to some overestimate of C_{ant} in deep and bottom waters [*Pardo et al*., 2014].

2.3. Net Community Production

Values of net community production (NCP), defined as the difference between net primary production and heterotrophic respiration, were obtained for each CTD profile by calculating the seasonal carbon and nitrate deficits from the surface to the T_{min} layer [*Le Corre and Minas*, 1983; *Jennings et al*., 1984] (see supporting information). This approach assumes no vertical or lateral mixing takes place in either the SML or with the underlying winter mixed-layer during the winter to summer period when the SML shoals. Continuous underway shipboard measurements of oxygen/argon (O_2/Ar) ratios [*Cassar et al*., 2007] using membrane inlet mass spectrometry (MIMS) [*Kaiser et al*., 2005] were also utilized for NCP estimates (see supporting information). The use of O_2/Ar ratios in the oceanic mixed layer provides a method to constrain biological processes (ΔO_2^{bio}) because oxygen and argon share similar physical solubility properties, but only oxygen is biologically consumed and produced. Additional measurements of underway surface oxygen concentration were made using an oxygen optode (accuracy of $\pm$ 2 μmol kg^{-1}; supporting information). The optode data were then combined with ΔO_2^{bio} (see supporting information), to partition total oxygen saturation (ΔO_2^{total}) into biological (the sum of photosynthesis and respiration) and physical (ΔO_2^{phys}) drivers (temperature changes, bubble injection, mixing) [*Cassar et al*., 2011] using:

$$\Delta O_2^{phys} = \Delta O_2^{total} - \Delta O_2^{bio} \quad (3)$$

While the MIMS technique provides an alternative estimate of NCP, the calculation of ΔO_2^{bio} using this method is complicated in high latitude waters due to a number of processes including ice melt, temperature change, and the entrainment of oxygen undersaturated waters into the SML that can lead to underestimates of ΔO_2^{bio} [e.g., *Castro-Morales et al*., 2013; *Cassar et al*., 2014; *Eveleth et al*., 2014]. Although these complications do provide challenges to interpretation of the O_2/Ar signals in our study region, the method does provide an alternative estimate of NCP and addresses different time scales (days to weeks) compared to the seasonal estimates based on carbon and nitrate deficits.

3. Results

3.1. Vertical Sections of Biogeochemical Properties

The mean property values for the water masses of the BROKE-West region are listed in Table 2. AASW, AABW, mCDW, and mSW were observed on all major CTD legs, CDW was not observed on Leg 1 and LSSW,

Table 2. Mean Values of Characteristic Properties in Each Water Mass in the BROKE-West Region

	AASW	CDW	mCDW	AABW	mSW	LSSW	DSW	ISW
γ_n (kg m^{-3})	27.75	28.00	28.19	28.34	28.29	28.34	28.51	28.23
θ (°C)	−1.01	1.74	0.48	−0.35	−0.11	−1.77	−1.89	−1.99
Salinity	34.21	34.69	34.68	34.66	34.67	34.49	34.56	34.46
O_2 (μmol kg^{-1})	275	174	193	208	204	278	280	283
DIC (μmol kg^{-1})	2187	2255	2251	2255	2257	2232	2237	2228
TA (μmol kg^{-1})	2291	2340	2340	2351	2350			
fCO_2 (μatm)	376	564	517	487	508	418	414	409
pH_{sws}	8.04	7.87	7.88	7.77	7.83	7.99	7.98	8.00
Ω_{ar}	1.33	1.04	0.96	0.50	0.72	1.15	1.09	1.17
NO_3^- (μmol kg^{-1})	28.03	32.08	31.59	31.85	31.67	30.17	30.15	29.81
PO_4^{2-} (μmol kg^{-1})	1.72	2.02	2.00	2.05	2.01	1.90	1.91	1.89
Si (μmol kg^{-1})	56.5	84.5	99.3	129.4	117.2	66.6	66.8	62.4
C_{ant} (μmol kg^{-1})		16	22	25	25	50	53	51

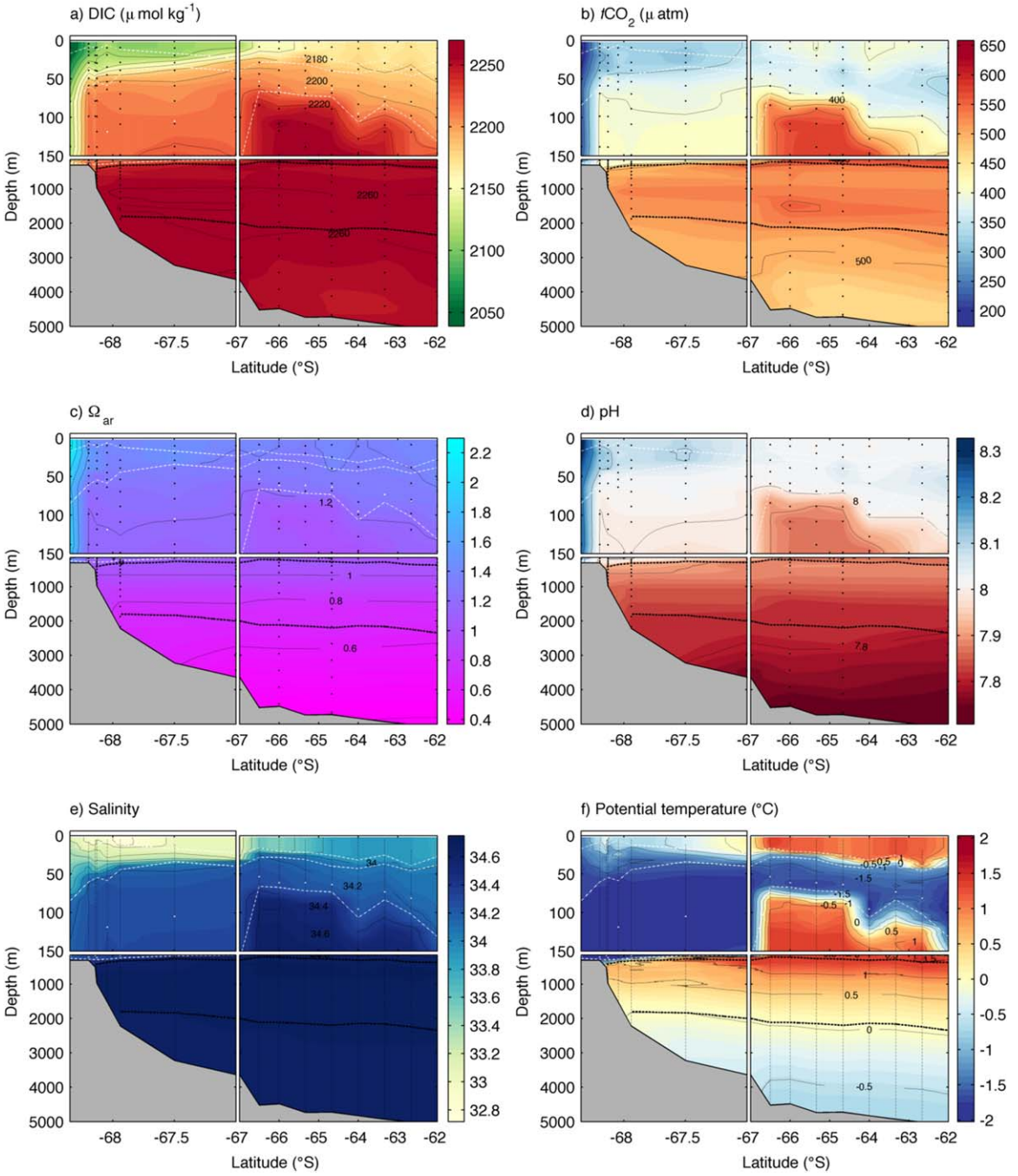

Figure 4. Leg 3 at 40°E, (a) DIC (μmol kg^{-1}), (b) fCO_2 (μatm), (c) saturation state of aragonite (Ω_{ar}), and (d) pH_{sws}, (e) salinity, and (f) potential temperature (°C). The black-dashed lines, on this and other similar plots, represent the (top) 28.03 kg m^{-3} and (bottom) the 28.27 kg m^{-3} neutral density surfaces that partly delineate major water masses in the study region. The black dots show the bottle and CTD locations. The white dots show the location of the T_{min} value and the white lines show the base of the (top) seasonal mixed layer, (middle) seasonal pycnocline, and (bottom) T_{min} layer. The marginal ice zone is indicated by a white rectangle at the surface toward the southern end of each leg. Scale changes are indicated by the breaks in the axis.

DSW, and ISW were only observed at the southern end of Leg 9. Here, we focus on the distribution of carbonate system parameters along sections in Legs 3 and 11 to illustrate the most important features exhibited in the study region with results from other legs described in the supporting information. The highest values of DIC and fCO_2 were at depth with Ω_{ar} and pH_{sws} values increasing toward the surface. AASW was the predominant water mass in the mostly ice-covered shelf waters at the southern end of Leg 3 (Figure 4). These AASW waters had the lowest observed DIC and calculated fCO_2 values of 2039 μmol kg^{-1} and 173

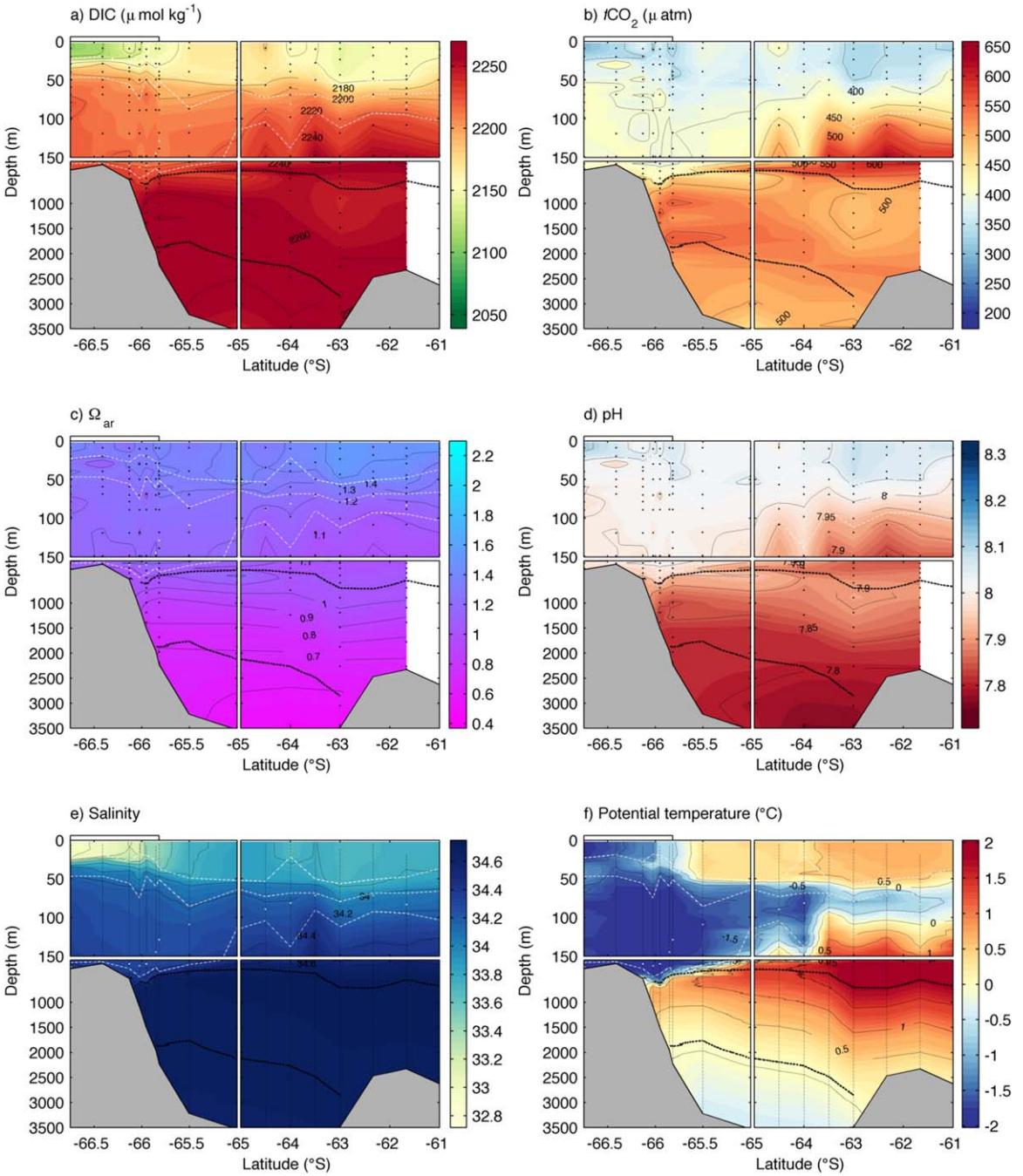

Figure 5. Leg 11, (a) DIC (μmol kg^{-1}), (b) fCO_2 (μatm), (c) saturation state of aragonite (Ω_{ar}), (d) pH_{sws}, (e) salinity, and (f) potential temperature (°C).

μatm, respectively, corresponding to Ω_{ar} and pH_{sws} values of 2.30 and 8.33, respectively. Further offshore, between 64°S and 66°S, water higher in DIC and fCO_2 shoals to around 100 m due to the upwelling of Warm Deep Water (WDW), a type of mCDW associated with the Weddell Gyre, as noted previously by *Williams et al*. [2010].

Leg 11 (Figure 5) in the eastern part of the study area, along with Leg 9 (see supporting information), are located in a different physical oceanographic regime when compared to the western CTD legs [*Meijers et al*., 2010]. Both of these eastern sections encompass the SB and the SACCF with intrusions of the ACC, which *Meijers et al*. [2010] identified by a rapid deepening of the 28.03 kg m^{-3} density surface north of ~64°S. At

the northern end of Leg 11, CDW protrudes over the southern edge of the Kerguelen Plateau and has the highest subsurface fCO_2 value of 659 μatm (station 103, depth 198 m). This coincides with a pocket of aragonite undersaturation ($\Omega_{ar} < 1$), a state where the dissolution of aragonite becomes thermodynamically favorable. Whilst the average depth of the aragonite saturation horizon ($\Omega_{ar} = 1$) across all sections is 711 $\pm$ 134 m (1 s.d.; $n = 38$), pockets of aragonite undersaturation at depths as shallow as 198 m occur near the base of the T_{min} layer toward the northern ends of Legs 7 and 11 ($\Omega_{ar} = 0.94$ and 0.99, respectively). The undersaturation coincides with stations that *Williams et al*. [2010] identified as locations of upwelling of relatively warm, O_2-depleted, nutrient, and carbon-rich mCDW/CDW into the surface layer (black dots on Figures 6–8, and 10b).

The distribution of biogeochemical properties in each of the deeper water masses showed little variation from east to west. *Meijers et al.* [2010] identified a decreasing temperature and salinity trend in sections from east to west, but no significant trends were observed in the CO_2 system properties for the same sections. The calculated mean fCO_2 of AABW varied between 500 $\pm$ 10 µatm (1 s.d.; $n = 10$) in Leg 9 to 481 $\pm$ 13 µatm (1 s.d.; $n = 30$) in Leg 1. The calculated AABW C_{ant} concentration was 25 $\pm$ 3 µmol kg^{-1} (1 s.d.; n = 127) across all sections. The water masses observed over the shelf (excluding AASW) were the most enriched in C_{ant}, with DSW being the highest at 53 $\pm$ 3 µmol kg^{-1} (1 s.d.; n = 3), although these shelf waters were only observed at the southern end of Leg 9.

3.2. Distribution of Sea-Air CO_2 Flux and Oxygen Saturation

The measured underway sea-surface values of fCO_2 varied between 187 and 411 μatm with the lowest values observed over the Antarctic shelf and slope in Zone 1 (Table 3) and north of the SACCF. The higher values were observed over a broad region that encompassed the eastern limb of the Weddell Gyre in Zone 2 and in a narrow band stretching further to the east and to the north of the Antarctic Slope Front. These broad features are visible in the underway measurements of ΔfCO_2, whereby negative values imply surface water conditions that are undersaturated with respect to the atmosphere (Figure 6a). The sea-air $CO_{2\ flux}$ (Figure 6b) shows a similar pattern to that of ΔfCO_2. However, the sea-air flux estimates are determined by a combination of the magnitude and sign of ΔfCO_2, the strength of the winds and sea-ice cover in the area. This is apparent near Mawson station (67.6027°S, 62.8738°E) where fCO_2 undersaturated waters, minimal sea-ice cover, and strong wind speeds of up to 30 m s^{-1} resulted in a maximum flux estimate of -221 mmol C m^{-2} d^{-1}. The mean CO_{2flux}^{uw} across the whole survey, based on the underway measurements, was -8 ± 21 mmol C m^{-2} d^{-1} (1 s.d.; $n = 59{,}375$). In comparison, the sea-air $CO_{2flux}^{ice-free}$ (Figure 6c) estimated for the ice-free period prior to sampling, varied from -0.48 and 0.62 mol C m^{-2}. Although our measurements are not made over a full year, the $CO_{2flux}^{ice-free}$ units are given in mol C m^{-2} to allow a comparison in section 4.1 with other yearly estimates of $CO_{2\ flux}$. The mean $CO_{2flux}^{ice-free}$ for the study area was 0.07 $\pm$ 0.13 mol C m^{-2} (1 s.d.; $n = 85$), indicating that the study area was a weak net source of CO_2 to atmosphere.

Surface water O_2 concentrations (ΔO_2^{total}) were supersaturated throughout most of the study area (Figure 7a). The greatest values of 22% supersaturation were observed over the shelf in the western part of the survey region. O_2 undersaturation was observed in small pockets on most transects, with the most significant regions of undersaturation observed in the MIZ on Leg 1 in the west, and a broad region of undersaturation just north of the shelf on Leg 8. The associated biological (ΔO_2^{bio}) and physical (ΔO_2^{phys}) changes from O_2/Ar data are shown in Figures 7b and 7c. *Eveleth et al*. [2014] suggested using their equation (5) to calculate ΔAr to assess the physical oxygen changes. Comparison with the method used in equation (3) of this paper, which assumes $[Ar]/[Ar]_{sat} = 1$, shows the two methods agree within 0.17 $\pm$ 0.14% for the entire duration of the study and indicates the Ar concentration was close to saturation values. The greatest difference observed was 1% in the MIZ in the far south of Leg 1, perhaps due to cooling of ice-melt that can lower Ar concentrations. The high values of biological undersaturation (Figure 7b) need not have been due to respiration in the SML and instead may reflect supply of low O_2 waters from below that can lead to measured values of O_2/Ar being less than the O_2/Ar ratio at saturation with the atmosphere [e.g., *Cassar et al*., 2014]. This would lead to underestimates of biological productivity, as discussed later in section 3.3, and therefore overestimate the contribution of ΔO_2^{phys} to the ΔO_2^{total} supersaturation observed throughout most of the study. However, ΔO_2^{phys} was typically within $\pm$ 3% with small pockets of undersaturation approaching 10% in ice-covered waters at the southern end of Leg 1.

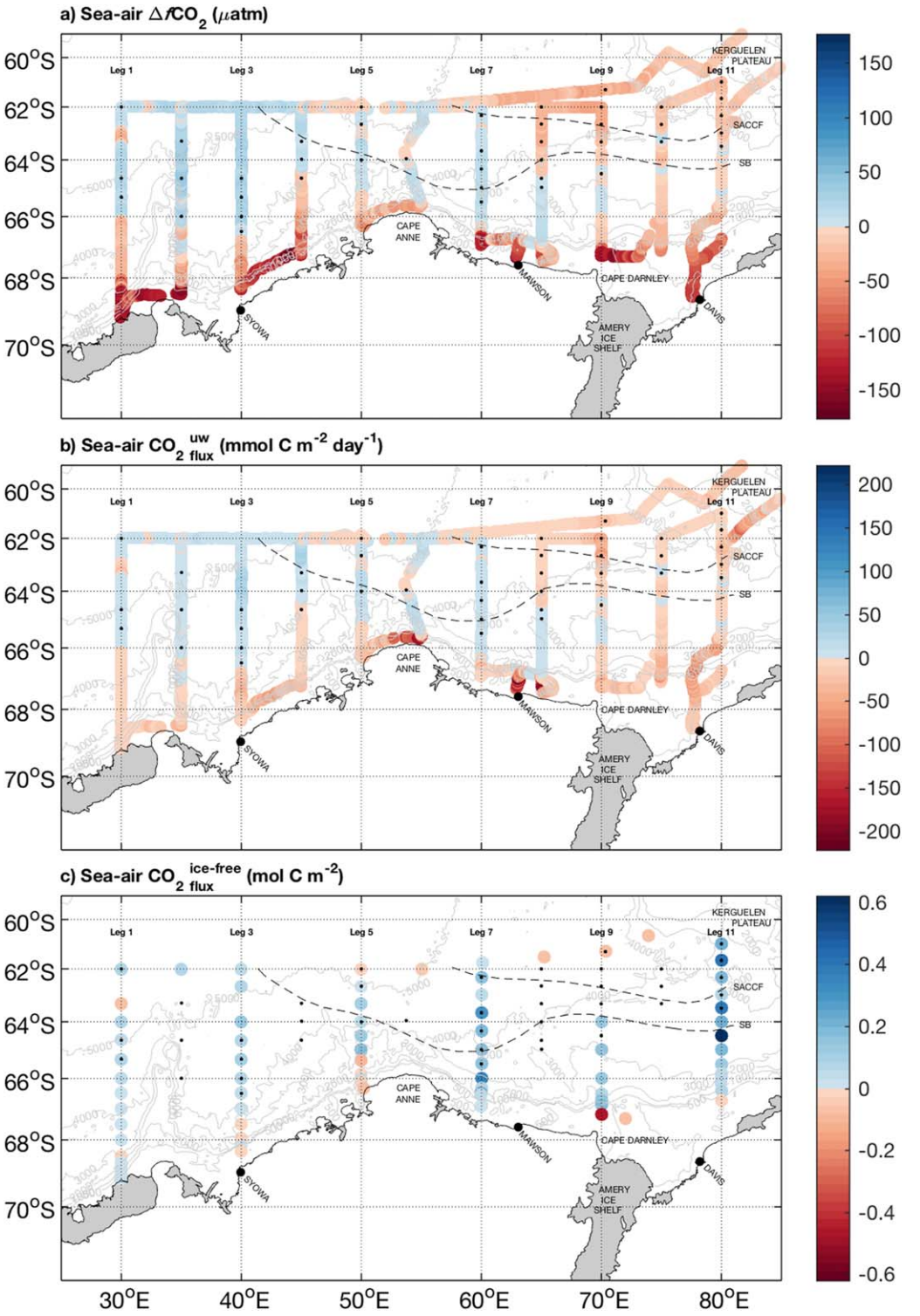

Figure 6. Underway surface measurements of, (a) sea-air ΔfCO_2 (μatm), (b) sea-air $CO_2{}^{uw}_{flux}$ (mmol C m^{-2} d^{-1}), and (c) sea-air $CO_2{}^{ice-free}_{flux}$ (mol C m^{-2}) estimates calculated from daily average CCMP wind speeds during each ice-free day prior to the ship's arrival on station. Positive sea-air flux values imply a net transfer from the ocean to the atmosphere. The small black dots, on this and other similar plots, represent the locations of surface layer upwelling zones as determined by positive anomalies of potential temperature at 100 m [*Williams et al.*, 2010].

3.3. Net Community Production

Seasonally integrated estimates of NCP, throughout the ice-free period prior to sampling, from both carbon (NCP_C) and nitrate (NCP_N) [*Pasquer et al.*, 2010] depletion profiles show distinct regions of biological

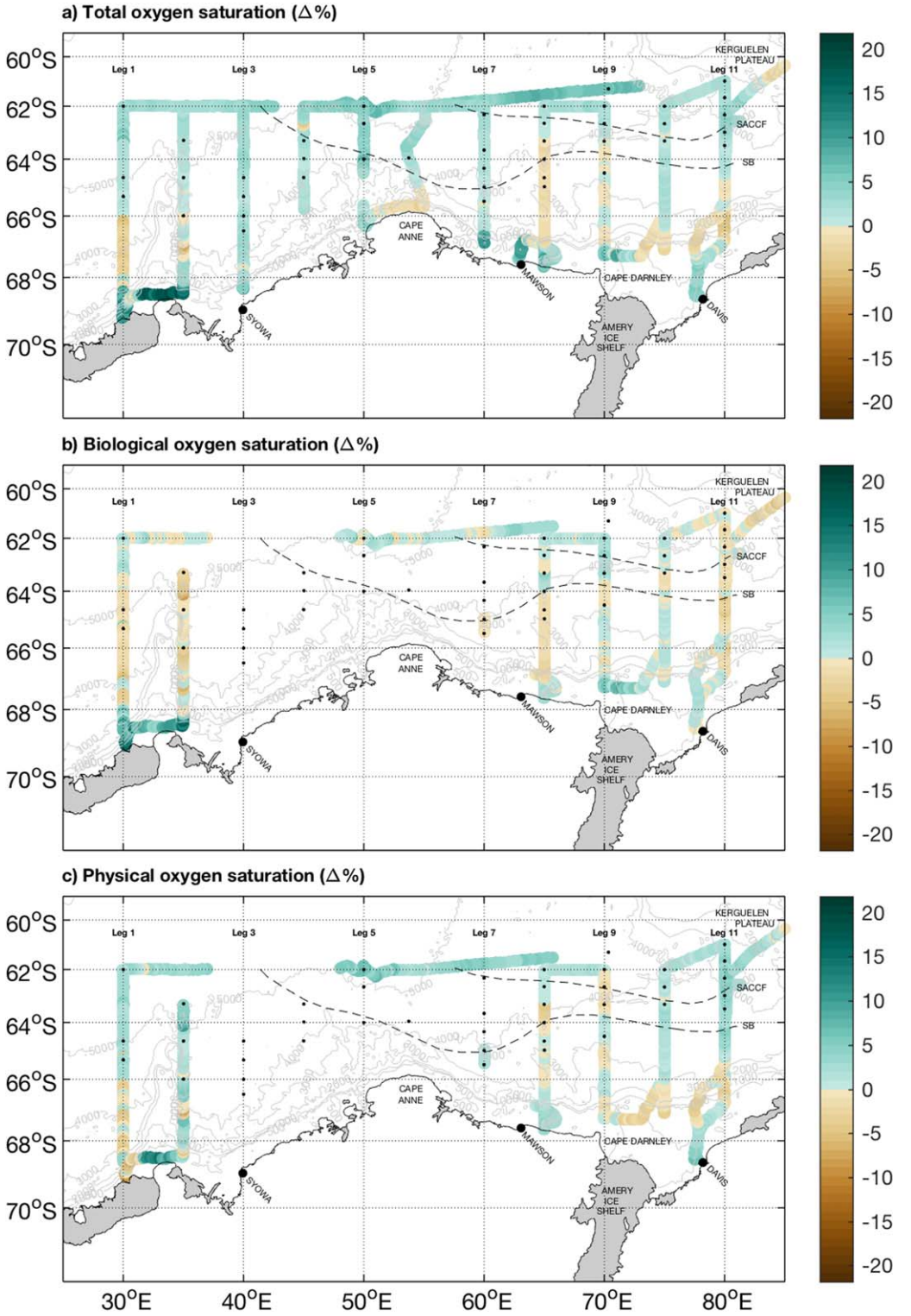

Figure 7. Distribution of, (a) total change in surface oxygen saturation (Δ%), (b) biological change in oxygen saturation (Δ%), and (c) physical change in oxygen saturation (Δ%) from underway measurements.

productivity (Figures 8a and 8b). NCP estimates as high as 6.4 and 6.0 mol C m^{-2} for carbon and nitrate, respectively, were observed near the Japanese research station, Syowa (69.00°S, 39.35°E), and over the shelf near Cape Darnley, Prydz Bay (70°E). Although the Kerguelen Plateau and the Antarctic shelf and slope

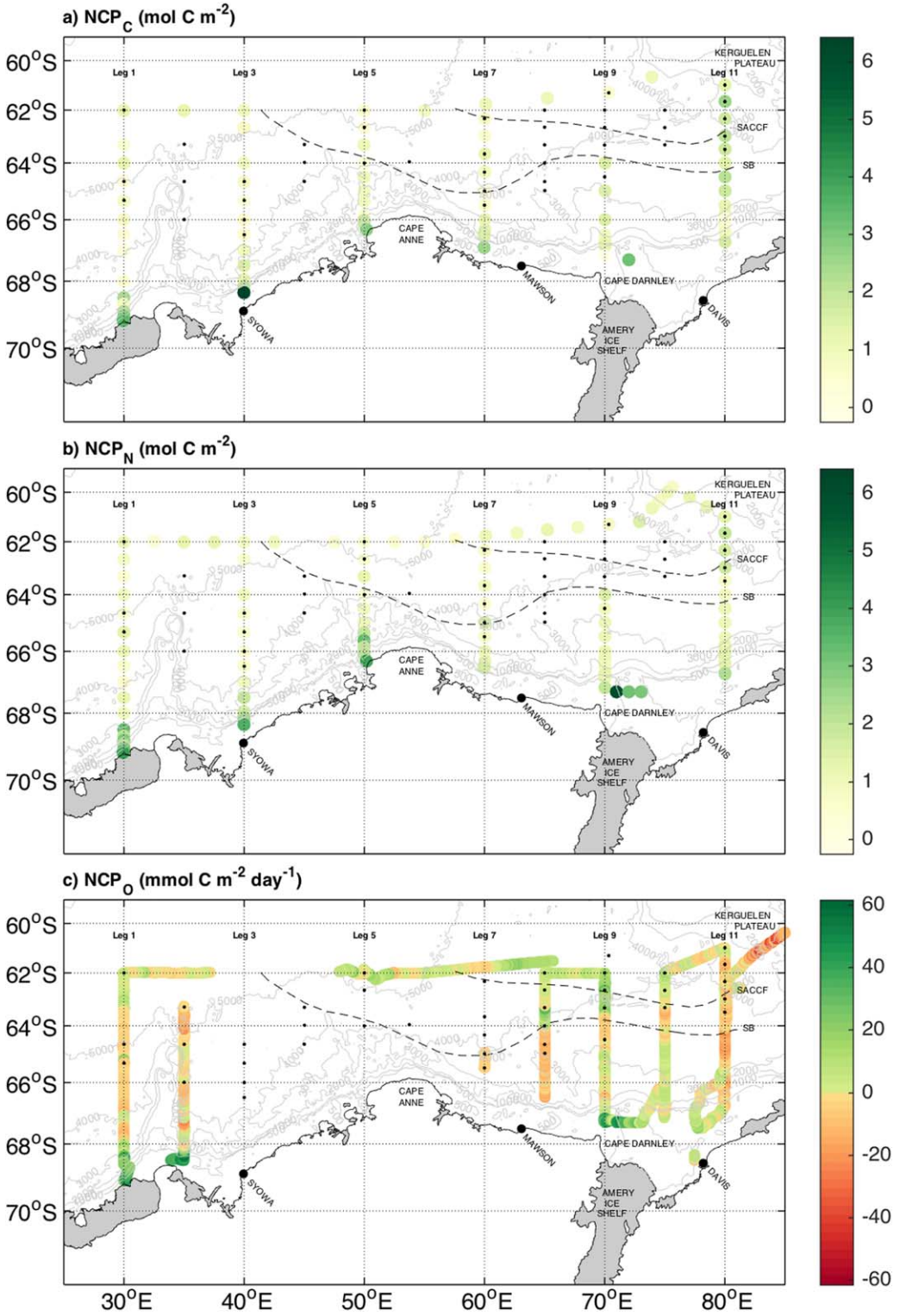

Figure 8. Net community production (NCP) estimates based on seasonally integrated (a) carbon (mol C m^{-2}), and (b) nitrate (mol C m^{-2}) deficits, and (c) underway O_2/Ar values (mmol C m^{-2} d^{-1}).

featured the highest rates of biological productivity, the majority of the survey area exhibited much lower values with a mean NCP_C of 1.3 ± 0.9 mol C m^{-2} (1 s.d.; $n = 81$) and NCP_N of 1.4 ± 0.9 mol C m^{-2} (1 s.d.; $n = 108$).

Table 3. Mean Surface Value Properties (± 1 s.d.) in Zones 1 (Continental Shelf/Slope), Zone 2 (Offshore West of ~45°E), and Zone 3 (offshore East of ~45°E)

	Zone 1	Zone 2	Zone 3
Temperature (°C)	−0.69 ± 0.63	0.67 ± 0.80	0.62 ± 0.30
fCO_2 (μatm)	300 ± 50	365 ± 20	348 ± 14
Ice-free days	28 ± 31	23 ± 16	56 ± 19
$CO_{2flux}^{ice-free}$ (mol C m^{-2})	0.03 ± 0.13	0.04 ± 0.04	0.14 ± 0.16
CO_{2flux}^{uw} (mmol C m^{-2} d^{-1})	−20 ± 28	3 ± 8	−6 ± 15
NCP_C (mol C m^{-2})	1.7 ± 1.2	0.8 ± 0.5	1.1 ± 0.6
NCP_N (mol C m^{-2})	2.1 ± 1.1	0.9 ± 0.6	0.9 ± 0.4
NCP_O (mmol C m^{-2} d^{-1})	5 ± 17	−1 ± 7	0 ± 10
F_e (mmol C m^{-2} d^{-1})	0.005 ± 0.005	0.006 ± 0.005	0.03 ± 0.02
F_v (mmol C m^{-2} d^{-1})	0.6 ± 0.1	0.44 ± 0.04	0.52 ± 0.07
ΔO_2^{total} (%)	3 ± 5	2 ± 2	2 ± 2
ΔO_2^{bio} (%)	2 ± 4	−1 ± 2	0 ± 1
ΔO_2^{phys} (%)	0 ± 3	1 ± 3	2 ± 2
C/N utilization ratio[a]	5.5 ± 2.3	5.9 ± 2.0	8.1 ± 3.1
C/Si utilization ratio[a]	2.5 ± 1.8	2.3 ± 1.2	1.5 ± 0.5
Si/N utilization ratio	3.0 ± 1.5	3.0 ± 1.1	5.7 ± 2.1

[a]Estimates corrected for sea-air CO_2 flux.

The daily estimates of NCP from the underway O_2/Ar system (NCP_O) showed more variability than the seasonally integrated estimates described above. There was some agreement in terms of the shelf being more productive (maximum NCP_O of 62 mmol C m^{-2} d^{-1}), although the NCP_O estimates also revealed broad regions of negative NCP values. The lowest of these values (−46 mmol C m^{-2} d^{-1}) was observed in the northeast sector of the study region and coincided with a senescent phytoplankton bloom (K. Westwood, personal communication, 2015) visible in Figure 2f as a modest concentration of chlorophyll-*a* averaged over the month of February. Whilst this may indicate a broad area of biological respiration (net heterotrophy), the upwelling of O_2 depleted water into the mixed layer could also influence these values, leading to underestimates of biological productivity in some areas and therefore incorrectly signal net heterotrophy in others. Other vertical processes, such as entrainment (F_e) and diffusion (F_v), have been accounted for in the O_2 mixed layer budget (see supporting information). The influence of entrainment was found, on average, to increase NCP_O estimates by ~1 %. This was due to the general shoaling of the mixed layer depth during the winter to summer transition, which would result in no change to the O_2 mixed layer budget. The influence of diffusion however, was found to be more significant, with NCP_O estimates increasing by up to ~40 % (Table 3).

4. Discussion

4.1. CO_2 Uptake and Storage

Biological activity over the shelf and slope during the summer resulted in surface fCO_2 values as much as 48% undersaturated with respect to the atmosphere, which produced uptake of CO_2 from the atmosphere in this region (Figures 6a and 6b). Underway measurements can bias net season flux estimates due to limited sampling in space and time. In order to assess the potential for bias, $CO_{2flux}^{ice-free}$ was also estimated for the period between sea-ice melt and when sampling occurred (Figure 6c). The premelt under ice conditions indicate most wintertime surface mixed-layer fCO_2 values were supersaturated with respect to the atmosphere (Figure 10a), consistent with other under-ice observations from within the study area and the Weddell Gyre [*Bakker et al*., 1997, 2008; *Bellerby et al*., 2004]. These $CO_{2flux}^{ice-free}$ estimates suggest that the study area as a whole was a net source of CO_2 to the atmosphere, albeit with uncertain significance. This uncertainty relates to the assumptions associated with the onset and development of biological productivity, the 20% error associated with the gas transfer velocity [*Wanninkhof*, 2014] and the effectiveness of sea-ice as a barrier to sea-air gas exchange [*Loose et al*., 2009].

Although the $CO_{2flux}^{ice-free}$ estimates suggested that the survey region was a net source of CO_2 to the atmosphere, areas of CO_2 uptake were observed, which was most enhanced over the shelf near Cape Darnley (−0.48 mol C m^{-2}). This is less than the uptake estimated for the Ross Sea by *Arrigo et al*. [2008a] (−1.7 to −4.2 mol C m^{-2} yr^{-1}), but is comparable to the uptake of −0.5 mol C m^{-2} yr^{-1} measured at a nearby coastal location in Prydz Bay [*Roden et al*., 2013], and is of similar magnitude to the uptake measured in the

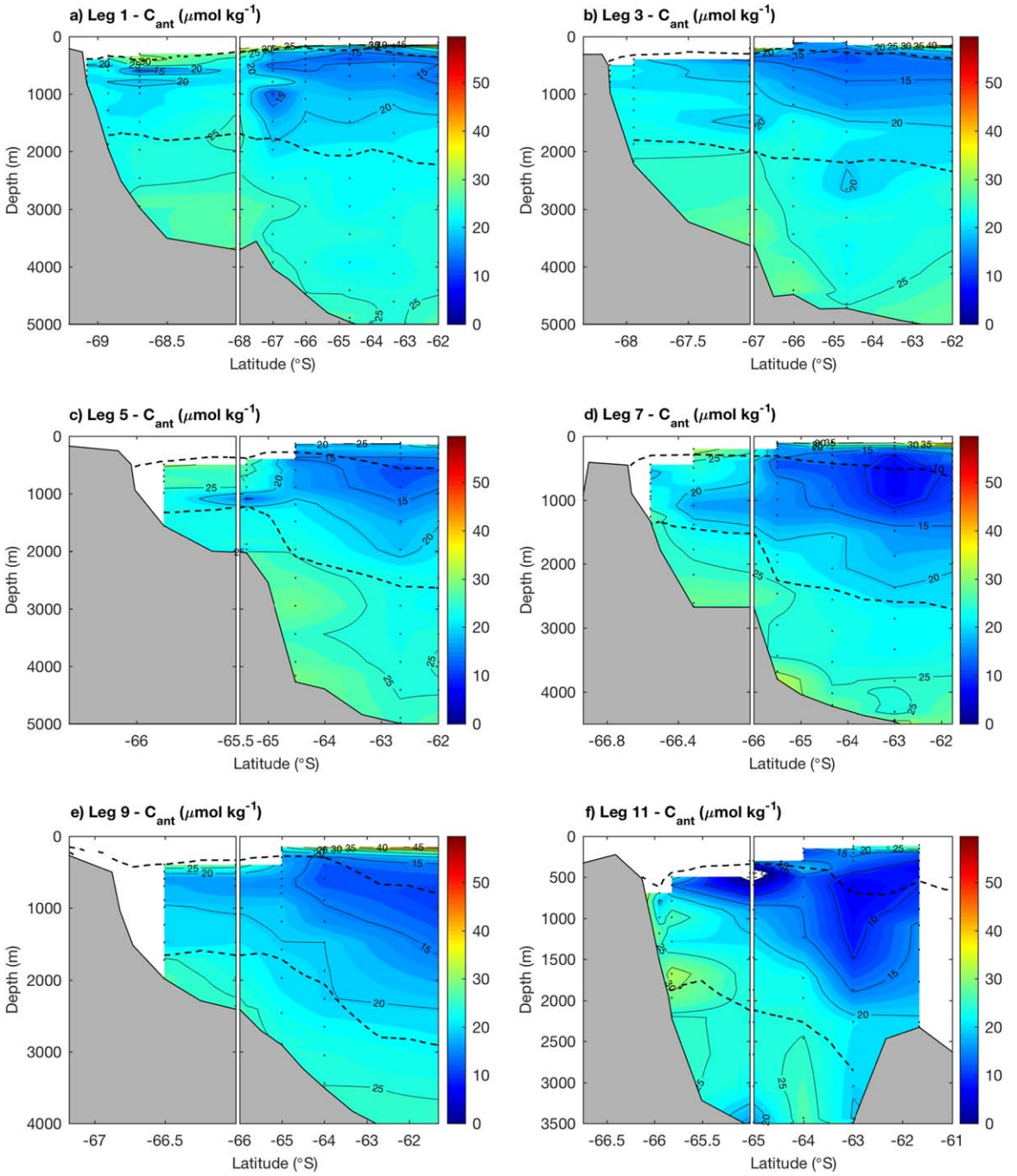

Figure 9. Anthropogenic carbon estimates (μmol kg^{-1}) for all sections, excluding surface water classified as AASW.

west Antarctic Peninsula [*Legge et al.*, 2015] and the Scotia Sea [*Jones et al.*, 2015]. Further offshore in Zone 2, both CO_{2flux}^{uw} and $CO_{2flux}^{ice-free}$ estimates show that the eastern limb of the Weddell Gyre was a net CO_2 source to the atmosphere. This area had a recent retreat of sea-ice (Table 3 and supporting information) and the net source here may be more indicative of under-ice conditions, before biologically induced reductions in fCO_2 could occur, as previously observed in this region [*Bakker et al.*, 2008; *Brown et al.*, 2015]. The various controls of surface water biogeochemical dynamics in the study area will be discussed later in section 4.2.

The high CO_2 uptake observed at the southern end of Leg 9 coincided with the highest concentrations of C_{ant}, which were observed in the underlying shelf waters (Table 2). The C_{ant} concentration of these

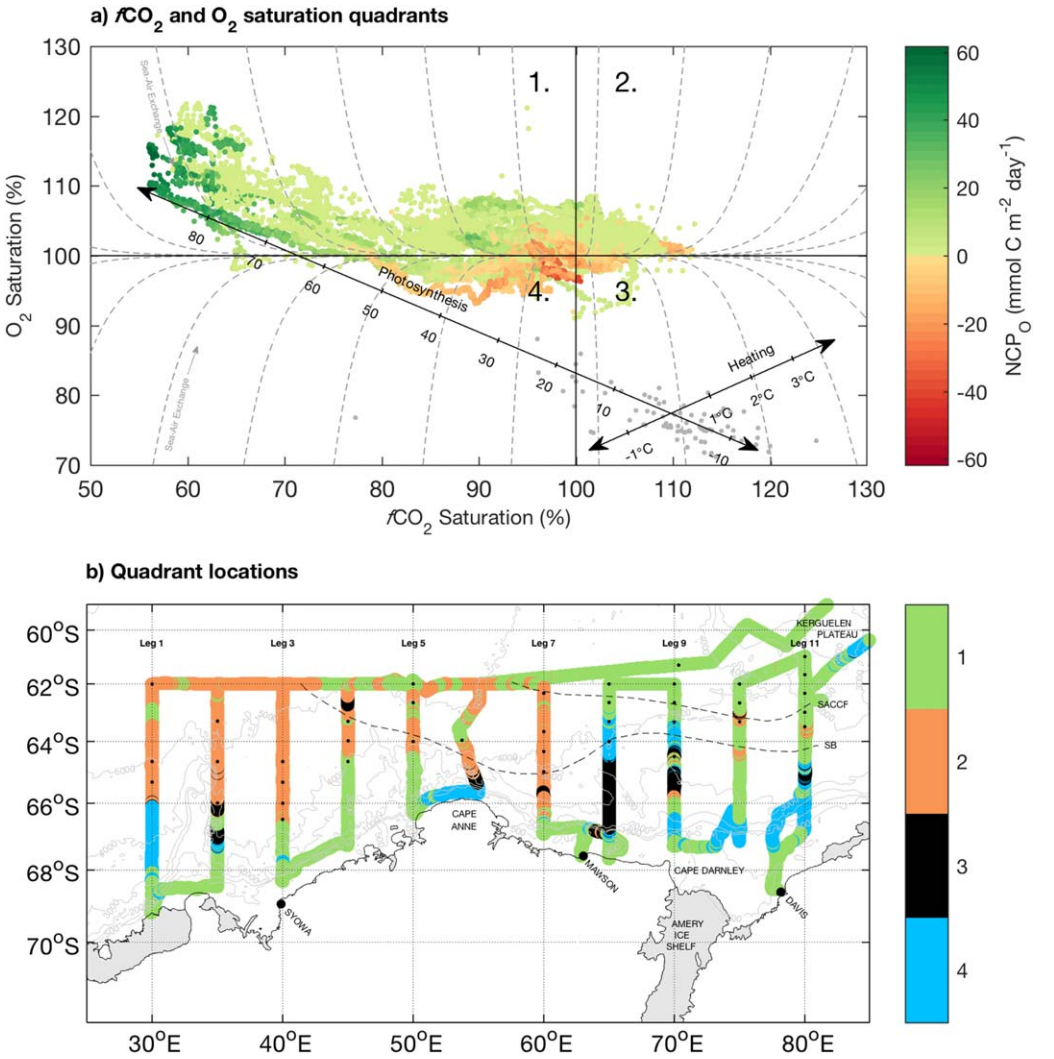

Figure 10. (a) Percentage saturation of fCO_2 versus the percentage saturation of O_2, colored with underway surface estimates of NCP (mmol C m^{-2} d^{-1}) from O_2/Ar ratios. Vertical and horizontal lines represent 100% saturation of fCO_2 and O_2. Based on these relationships the figure is separated into quadrants, whereby each quadrant represents changes dominated by (1) photosynthesis, (2) warming, (3) respiration or upwelling, and (4) cooling. The process vectors centered on the mean wintertime saturation state for each gas (grey dots; taken from the T_{min} layer) represent the production of O_2 and consumption of CO_2 at a theoretical photosynthetic quotient of −0.7 with overlaid NCP (mmol C m^{-2} d^{-1}) values based on an average MLD and ice-free day period of 40 m and 37 days, respectively. The second process vector represents changes in saturation caused by 1°C of warming/cooling (ΔO_2 sat = 2.64% $°C^{-1}$ and ΔfCO_2 sat = 4.23% $°C^{-1}$). The dashed lines represent the O_2 and fCO_2 saturation values based on a model of sea-air exchange [see *Carrillo et al.*, 2004]. (b) The spatial distribution of the quadrants.

shelf waters was similar to the TrOCA based C_{ant} value of 44 μmol kg^{-1} estimated by *Shadwick et al.* [2014] for DSW in the Mertz Polynya region of East Antarctica. Whilst DSW was only observed in one location in the BROKE-West study region, its presence is significant as it is a precursor for the formation of AABW, which originates in specific regions around Antarctica and sinks to abyssal depths due to varying combinations of brine rejection from sea-ice formation and ocean/ice-shelf interactions. In doing so, it contributes significantly to the global overturning circulation and sequesters heat and atmospheric gases to the deep ocean [*Orsi et al.*, 1999; *Johnson*, 2008; *Marshall and Speer*, 2012]. No areas of AABW production were identified during the summertime BROKE-West study [*Williams et al.*, 2010]. However, a significant site of AABW production was recently discovered in the Cape Darnley region near the southern end of Leg 9 [*Ohshima et al.*, 2013; *Williams et al.*, 2016]. The westward flow of AABW that is observed high on the continental slope between Legs 5 and 7, as noted previously by *Meijers et al.* [2010], could therefore represent recently formed AABW from the Cape Darnley region that is moving downslope and deflected westward [*Gill*, 1973].

The higher temperature, salinity, and fCO_2 and lower oxygen values of AABW to the east of Cape Darnley, relative to the west, indicates a greater elapsed time since formation and hence greater mixing with the warmer and more saline overlying mCDW and CDW [*Meijers et al*., 2010]. Given the formation of AABW at Cape Darnley and its subsequent transport west, we might also expect to see higher C_{ant} concentrations in the western CTD legs (Figure 9), although no significant trend in AABW C_{ant} concentration was observed. Furthermore, the high values of C_{ant} in AABW may in part reflect the tendency toward overestimation of C_{ant} in deep waters by the TrOCA method [*Pardo et al*., 2014]. Nonetheless, it is likely that high C_{ant} values observed in the shelf waters of the Cape Darnley region contribute anthropogenic CO_2 to AABW.

The complex role of high-latitude Southern Ocean waters in the global climate system makes its future response to projected climate forcing extremely difficult to model [*Meijers*, 2014]. As such, predicting the future uptake and storage of CO_2 in the SIZ of East Antarctica is beyond the scope of this paper. Particularly as change and variability in East Antarctic sea-ice seasonality comprises mixed signals on regional to local scales [*Massom et al*., 2013; *Hobbs et al*., 2016]. In contrast, the west Antarctic Peninsula has experienced a rapid reduction in sea-ice cover in recent years [*Stammerjohn et al*., 2008; *Li et al*., 2014], although as yet, no significant long-term trends in carbonate system parameters have been detected as a result [*Hauri et al*., 2015]. Sea-ice can influence sea-air CO_2 exchange by acting as a physical barrier to sea-air gas exchange itself [*Semiletov et al*., 2004; *Zemmelink et al*., 2006; *Miller et al*., 2011; *Nomura et al*., 2013] and by controlling mixed layer development and the subsequent availability of light and nutrients [*Venables et al*., 2013]. This was observed by *Geibert et al*. [2010] in the eastern boundary of the Weddell Gyre who found that the cumulative melting of both sea-ice and icebergs provided a steady source of iron that sustained biological productivity and therefore influenced the sea-air gradient in CO_2.

The present synergy between winter sea-ice cover and summer biological productivity, particularly over the shelf, acts to reduce the flux of CO_2 from deep waters to the atmosphere in the BROKE-West study region. This seasonal synergy has been previously described in Arctic waters as a rectification process (i.e., one that emphasizes uptake by biological processes in summer and minimizes outgassing by physical processes in winter) [*Yager et al*., 1995]. To examine how this seasonal ice cover might influence the uptake of CO_2 by the surface waters in the BROKE-West region, we compared the *n*DIC concentration measured in the T_{min} layer by *Ishii et al*. [1998] during the austral summer of 1992/1993 with values measured in this study. Values from the T_{min} layer are used as a reference level and to minimize the potential to bias the results due to the seasonal drawdown of carbon in spring and summer. Using a Revelle factor [*Revelle and Suess*, 1957] of 16.4 and an atmospheric growth rate in fCO_2 of ~1.9 μatm yr^{-1}, the expected increase in DIC of surface waters in the region would be 0.66 μmol kg^{-1} yr^{-1}, or 8.52 μmol kg^{-1} from 1993 to 2006. Our average *n*DIC concentration from the T_{min} layer for the entire survey area was 2206 ± 8 μmol kg^{-1} (1 s.d.; $n = 87$) compared to the 1992/1993 value of 2197 ± 4 μmol kg^{-1} (1 s.d.; $n = 14$), which represents an increase in DIC of 9 μmol kg^{-1}. Variations in biological productivity or increased upwelling during this time could also be responsible for the increase in *n*DIC, however, a comparison of the mean *n*N values between our study and 1992/1993 showed no significant change ($nN_{1992/1993} = 28.7 \pm 0.7$ μmol kg^{-1} (1 s.d.; $n = 14$); $nN_{2006} = 29.5 \pm 1$ μmol kg^{-1} (1 s.d.; $n = 108$)), which suggests that surface waters in the SIZ of the BROKE-West region are tracking the atmospheric increase in fCO_2. A similar trend was observed by *van Heuven et al*. [2014] in the western Weddell Sea, suggesting that sea-ice cover in these locations, does not constitute a major impediment for sea-air CO_2 equilibration on annual time scales.

4.2. Surface Water Biogeochemical Cycling

Concurrent measurements of dissolved O_2 and carbon parameters can help constrain understanding of controls on surface ocean carbon dynamics [*Bender et al*., 2000; *Álvarez et al*., 2002]. For example, a detection of fCO_2 undersaturation and O_2 supersaturation, with respect to the atmosphere, would imply photosynthesis as a controlling mechanism, whereas fCO_2 supersaturation and O_2 undersaturation would indicate a source of net respiration or mixing with deeper waters below the SML. *Carrillo et al*. [2004] utilized this approach in the west Antarctic Peninsula by segregating measurements of O_2 and fCO_2 into one of four classifications. This was done based on the saturation state of each gas relative to the atmosphere, which allowed each classification to represent changes in gas concentration that were dominated by either physical or biological processes.

The incorporation of NCP values from underway O_2/Ar measurements provides further insights into the processes influencing the O_2 and fCO_2 distributions (Figure 10a). Each classification, or quadrant, partitions the underway-surface observations into changes driven predominantly by (1) photosynthesis, (2) warming, (3) net respiration/deep mixing, and (4) cooling, with the highest NCP_O values being associated with photosynthesis. Deviations from these theoretical relationships, illustrated by the process vectors in Figure 10a, may result from the different sea-air exchange rates for O_2 and fCO_2 (see model of sea-air exchange in Figure 10a) with timescales that range from days to weeks for O_2 and months for fCO_2 [*Broecker and Peng*, 1982], or from the formation and dissolution of calcium carbonate [*Dieckmann et al*., 2008]. Plotting the spatial distribution of each data point based on its quadrant classification (Figure 10b) reveals distinct regions where these biological and physical processes appear to dominate.

Two processes in particular, warming and photosynthesis, can explain much of the observed variability in O_2 and fCO_2 saturation during the BROKE-West study, accounting for 31% and 49% of the observed values, respectively. Those waters that were dominated by surface warming, resulting in decreased gas solubility, are associated with the relatively warmer waters of the Weddell Gyre in the northwest sector of the study area (Figures 2h and 2i), which agrees with the findings of *Nomura et al*. [2014] who found a similar temperature control on surface fCO_2 values in this region. The variability driven by photosynthesis occurs over the shelf and slope with a second region observed offshore, north of the SACCF. Regions where photosynthesis appears to be the dominant mode of O_2 and fCO_2 variability, i.e., quadrant 1, also show elevated satellite chlorophyll-*a* concentrations, which often indicate intense phytoplankton blooms, particularly near the sea-ice edge and within Prydz Bay (Figures 2e and 2f). Surface data associated with quadrant 3, which only accounted for 5% of the observations, may indicate areas of localized upwelling or net respiration from biological activity. For example, the broad quadrant 3 classification observed in Leg 8 correlates well with both the biological O_2 undersaturation observed in Figure 7b and the positive 100 m temperature anomalies, indicative of upwelling, at two of the xCTD stations [*Williams et al*., 2010]. Data associated with quadrant 4 (cooling) accounts for 15% of the observations and correlates well with areas of marginal sea-ice (Figures 2b and 2c), which suggests that an increase in gas solubility driven by cold sea-ice melt water may cause the observed variability in these areas.

The distribution of surface water biogeochemical properties shows distinct regional characteristics, which generally agree with the zones outlined by *Schwarz et al*. [2010]. Table 3 summarizes the mean values of selected parameters based on this classification scheme. However, when NCP is considered over seasonally integrated time-scales (Figures 8a and 8b), only two distinct regions are apparent. These observations reveal that the majority of the study area experienced relatively low biological productivity at the time of sampling, with the exception of waters over the continental shelf and moderate productivity near the Kerguelen Plateau. Although iron was not directly measured during the study, there are various lines of evidence to suggest that biological activity was limited by its supply to the surface mixed layer. These include phytoplankton species composition and chlorophyll degradation products measured by *Wright et al*. [2010] and the utilization ratios of macronutrients (Table 3), whose individual concentrations were never below limiting levels [*Westwood et al*., 2010]. *Wright et al*. [2010] further postulated that grazing on the phytoplankton bloom and export of faecal pellets stripped the upper water column of iron, creating a southward migrating iron gradient that followed the retreat of the melting sea-ice, thus limiting phytoplankton growth in the upper water column. Our seasonally integrated estimates of NCP do not resolve this pattern of biological activity, however, our results suggest that the supply of iron over the shelf, through a variety of mechanisms, may have been sufficient to sustain high levels of biological activity throughout most of the summer period.

5. Conclusions

In this study of the biogeochemical dynamics in the seasonal sea-ice zone of East Antarctica, distinct regions of biological activity and sea-air CO_2 flux were found. Estimates of the CO_2 flux since the retreat of sea-ice prior to the survey suggest that the entire study area is a weak net source of CO_2 to the atmosphere. Waters over the shelf and north of the SACCF were generally sites of oceanic CO_2 uptake. This uptake, particularly over the shelf/slope, was driven by strong biological productivity as observed in NCP estimates that were as high as 6.4 mol C m^{-2}. Although micronutrients were not measured, it is likely that this strong biological

productivity was sustained through their supply. The largest CO_2 uptake was observed near Cape Darnley and the magnitude of the CO_2 sink is commensurate with other coastal and shelf based estimates of CO_2 uptake, both in East Antarctica and along the west Antarctic Peninsula. Further offshore, in the western sector of the study area, the warmer waters of the Weddell Gyre-dominated surface water biogeochemical dynamics, reducing gas solubility and causing a broad region of CO_2 outgassing.

Wintertime under-ice estimates of fCO_2 indicate that the majority of the surface waters in the BROKE-West study region were supersaturated with respect to the atmosphere. The seasonal synergy between winter sea-ice cover and biological productivity during the summer however, acts to reduce the flux of CO_2 to the atmosphere, highlighting the important role that sea-ice plays in the biogeochemical dynamics of the region. Because the observed changes to the East Antarctic sea-ice are complex and are comprised of mixed signals on regional to local scales, making predictions about the future CO_2 source/sink nature of the SIZ is difficult. This is highlighted by the large variability in the drivers and timing of carbon cycling dynamics in this region. As such, the future CO_2 uptake or outgassing in the study area will most likely depend on the response of the solubility and biological pumps to: (1) changes in sea-ice seasonality and (2) the enhanced ventilation of carbon and nutrient-rich deep water driven by strengthening winds over the Southern Ocean.

Acknowledgments

NR was supported by an Australian Postgraduate Award and a CSIRO Oceans and Atmosphere scholarship. The collection and analyses of samples for this paper were supported by the Antarctic Climate and Ecosystem Cooperative Research Centre, the Australian Climate Change Research Program, and the Australian Scientific Assessment Committee Project 1302, awarded to B.T. The authors would like to thank Kristina Paterson, Ty Hibberd, Mark Pretty, and Kate Berry for carbon sampling and analysis as well as the officers and crew aboard the *RV Aurora Australis* for their professionalism and efforts. Professors Michael Bender and Nicolas Cassar, who helped establish O_2/Ar measurements on the ship, provided O_2/Ar ratio measurements on discrete samples used to calibrate the MIMS. The authors would also like to thank Doctor Elizabeth Jones and one anonymous reviewer for their thoughtful comments. Data availability: Underway carbon data are available from the Surface Ocean CO_2 Atlas at http://www.socat.info. CTD data are available from the Australian Antarctic Data Centre at http://data.aad.gov.au/aadc/metadata/metadata_redirect.cfm?md=/AMD/AU/BROKE-West_CTD_au0603. Data from the Princess Elizabeth Trough and WOCE SR3 transect available from the GLODAPv2 database at: http://cdiac.ornl.gov/oceans/GLODAPv2. MODIS-Aqua data obtained from the NASA Goddard Space Flight Center, Ocean Ecology Laboratory, Ocean Processing Group http://oceandata.sci.gsfc.nasa.gov/MODIS-Aqua/Mapped/Monthly/9km. NCEP-DOE Reanalysis 2 data provided by the NOAA/OAR/ESRL PSD available from: http://www.esrl.noaa.gov/psd/data/gridded/data.ncep.reanalysis2.html.

References

Álvarez, M., A. F. Rĭos, and G. Rosón (2002), Spatio-temporal variability of air–sea fluxes of carbon dioxide and oxygen in the Bransfield and Gerlache Straits during Austral summer 1995–96, *Deep Sea Res., Part II*, *49*(4–5), 643–662, doi:10.1016/S0967-0645(01)00116-3.

Arrigo, K. R., G. van Dijken, and M. Long (2008a), Coastal Southern Ocean: A strong anthropogenic CO_2 sink, *Geophys. Res. Lett.*, *35*, L21602, doi:10.1029/2008GL035624.

Arrigo, K. R., G. L. van Dijken, and S. Bushinsky (2008b), Primary production in the Southern Ocean, 1997-2006, *J. Geophys. Res.*, *113*, C08004, doi:10.1029/2007JC004551.

Atlas, R., R. N. Hoffman, J. Ardizzone, S. M. Leidner, J. C. Jusem, D. K. Smith, and D. Gombos (2011), A cross-calibrated, multiplatform ocean surface wind velocity product for meteorological and oceanographic applications, *Bull. Am. Meteorol. Soc.*, *92*(2), 157–174, doi:10.1175/2010BAMS2946.1.

Bakker, D. C. E., H. J. W. de Baar, and U. V. Bathmann (1997), Changes of carbon dioxide in surface waters during spring in the Southern Ocean, *Deep Sea Res., Part II*, *44*(1–2), 91–127, doi:10.1016/S0967-0645(96)00075-6.

Bakker, D. C. E., M. Hoppema, M. Schröder, W. Geibert, and H. J. W. de Baar (2008), A rapid transition from ice covered CO_2–rich waters to a biologically mediated CO_2 sink in the eastern Weddell Gyre, *Biogeosciences*, *5*(5), 1373–1386, doi:10.5194/bg-5-1373-2008.

Bates, N. R., D. A. Hansell, C. A. Carlson, and L. I. Gordon (1998), Distribution of CO_2 species, estimates of net community production, and air-sea CO_2 exchange in the Ross Sea polynya, *J. Geophys. Res.*, *103*(C2), 2883–2896, doi:10.1029/97JC02473.

Bellerby, R. G. J., M. Hoppema, E. Fahrbach, H. J. W. de Baar, and M. H. C. Stoll (2004), Interannual controls on Weddell Sea surface water fCO_2 during the autumn–winter transition phase, *Deep Sea Res., Part I*, *51*(6), 793–808, doi:10.1016/j.dsr.2004.01.002.

Bender, M., J. Orchardo, M.-L. Dickson, R. Barber, and S. Lindley (1999), In vitro O_2 fluxes compared with ^{14}C production and other rate terms during the JGOFS Equatorial Pacific experiment, *Deep Sea Res., Part I*, *46*(4), 637–654, doi:10.1016/S0967-0637(98)00080-6.

Bender, M. L., M.-L. Dickson, and J. Orchardo (2000), Net and gross production in the Ross Sea as determined by incubation experiments and dissolved O_2 studies, *Deep Sea Res., Part II*, *47*(15–16), 3141–3158, doi:10.1016/S0967-0645(00)00062-X.

Boyd, P. W., and D. Mackie (2008), Comment on "The Southern Ocean biological response to aeolian iron deposition", *Science*, *319*(5860), 159, doi:10.1126/science.1149884.

Brewer, P. G., and J. C. Goldman (1976), Alkalinity changes generated by phytoplankton growth, *Limnol. Oceanogr.*, *21*(1), 108–117, doi:10.4319/lo.1976.21.1.0108.

Broecker, W. S., and T.-H. Peng (1982), *Tracers in the Sea*, Lamont-Doherty Geol. Obs., Palisades, N. Y.

Brown, P. J., et al. (2015), Carbon dynamics of the Weddell Gyre, Southern Ocean, *Global Biogeochem. Cycles*, *29*, 288–306, doi:10.1002/2014GB005006.

Cai, W.-J., and Y. Wang (1998), The chemistry, fluxes, and sources of carbon dioxide in the estuarine waters of the Satilla and Altamaha Rivers, Georgia, *Limnol. Oceanogr.*, *43*(4), 657–668, doi:10.4319/lo.1998.43.4.0657.

Carrillo, C. J., R. C. Smith, and D. M. Karl (2004), Processes regulating oxygen and carbon dioxide in surface waters west of the Antarctic Peninsula, *Mar. Chem.*, *84*(3–4), 161–179, doi:10.1016/j.marchem.2003.07.004.

Cassar, N., M. L. Bender, B. A. Barnett, S. Fan, W. J. Moxim, H. Levy, and B. Tilbrook (2007), The Southern Ocean biological response to aeolian iron deposition., *Science*, *317*(5841), 1067–1070, doi:10.1126/science.1144602.

Cassar, N., P. J. DiFiore, B. A. Barnett, M. L. Bender, A. R. Bowie, B. Tilbrook, K. Petrou, K. J. Westwood, S. W. Wright, and D. Lefevre (2011), The influence of iron and light on net community production in the Subantarctic and Polar Frontal Zones, *Biogeosciences*, *8*(2), 227–237, doi:10.5194/bg-8-227-2011.

Cassar, N., C. D. Nevison, and M. Manizza (2014), Correcting oceanic O_2/Ar-net community production estimates for vertical mixing using N_2O observations, *Geophys. Res. Lett.*, *41*, 8961–8970, doi:10.1002/2014GL062040.

Castro-Morales, K., N. Cassar, D. R. Shoosmith, and J. Kaiser (2013), Biological production in the Bellingshausen Sea from oxygen-to-argon ratios and oxygen triple isotopes, *Biogeosciences*, *10*(4), 2273–2291, doi:10.5194/bg-10-2273-2013.

Cavalieri, D. J., C. L. Parkinson, P. Gloersen, and H. Zwally (2015), Sea ice concentration from Nimbus-7 SMMR and DMSP SSM/I-SSMIS passive microwave data, Version 1, NASA Natl. Snow Ice Data Cent. Distrib. Act. Arch. Cent. [Available at http://dx.doi.org/10.5067/8GQ8LZQVL0VL, accessed 3 June.]

Copin-Montegut, C. (1988), A new formula for the effect of temperature on the partial pressure of CO_2 in seawater, *Mar. Chem.*, *25*(1), 29–37, doi:10.1016/0304-4203(88)90012-6.

Culberson, C. H., G. Knapp, M. C. Stalcup, R. T. Williams, and F. Zemlyak (1991), *A Comparison of Methods for the Determination of Dissolved Oxygen in Seawater*, WOCE Hydrogr. Programme Off., Woods Hole Oceanogr. Inst., Woods Hole, Mass.

Davidson, A. T., F. J. Scott, G. V. Nash, S. W. Wright, and B. Raymond (2010), Physical and biological control of protistan community composition, distribution and abundance in the seasonal ice zone of the Southern Ocean between 30 and 80°E, *Deep Sea Res., Part II*, *57*(9–10), 828–848, doi:10.1016/j.dsr2.2009.02.011.

de Baar, H. J. W., J. T. M. de Jong, D. C. E. Bakker, B. M. Löscher, C. Veth, U. Bathmann, and V. Smetacek (1995), Importance of iron for plankton blooms and carbon dioxide drawdown in the Southern Ocean, *Nature*, *373*(6513), 412–415, doi:10.1038/373412a0.

Dickson, A. G., and F. J. Millero (1987), A comparison of the equilibrium constants for the dissociation of carbonic acid in seawater media, *Deep Sea Res., Part A*, *34*(10), 1733–1743, doi:10.1016/0198-0149(87)90021-5.

Dickson, A. G., C. L. Sabine, and J. R. Christian (Eds.) (2007), *Guide to Best Practices for Ocean CO2 Measurements, PICES Spec. Publ. 3*, 191 pp., North Pacific Marine Science Organisation, Sidney BC, Canada.

Dieckmann, G. S., G. Nehrke, S. Papadimitriou, J. Göttlicher, R. Steininger, H. Kennedy, D. Wolf-Gladrow, and D. N. Thomas (2008), Calcium carbonate as ikaite crystals in Antarctic sea ice, *Geophys. Res. Lett.*, *35*, L08501, doi:10.1029/2008GL033540.

Dlugokencky, E. J., P. M. Lang, K. A. Masarie, A. M. Crotwell, and M. J. Crotwell (2015), Atmospheric carbon dioxide dry air mole fractions from the NOAA ESRL Carbon Cycle Cooperative Global Air Sampling Network, 1968-2014, Version: 2015-08-03. [Available at http://aftp.cmdl.noaa.gov/data/trace_gases/co.]

Eveleth, R., M.-L. Timmermans, and N. Cassar (2014), Physical and biological controls on oxygen saturation variability in the upper Arctic Ocean, *J. Geophys. Res. Oceans*, *119*, 7420–7432, doi:10.1002/2014JC009816.

Foldvik, A., and T. Gammelsrød (1988), Notes on Southern Ocean hydrography, sea-ice and bottom water formation, *Palaeogeogr. Palaeoclimatol. Palaeoecol.*, *67*(1–2), 3–17, doi:10.1016/0031-0182(88)90119-8.

García, H. E., and L. I. Gordon (1992), Oxygen solubility in seawater: Better fitting equations, *Limnol. Oceanogr.*, *37*(6), 1307–1312, doi:10.4319/lo.1992.37.6.1307.

García, H. E., and L. I. Gordon (1993), Erratum: Oxygen solubility in seawater: Better fitting equations, *Limnol. Oceanogr.*, *38*(3), 656.

Geibert, W., et al. (2010), High productivity in an ice melting hot spot at the eastern boundary of the Weddell Gyre, *Global Biogeochem. Cycles*, *24*, GB3007, doi:10.1029/2009GB003657.

Gibson, J. A. E., and T. W. Trull (1999), Annual cycle of fCO_2 under sea-ice and in open water in Prydz Bay, East Antarctica, *Mar. Chem.*, *66*(3–4), 187–200, doi:10.1016/S0304-4203(99)00040-7.

Gill, A. E. (1973), Circulation and bottom water production in the Weddell Sea, *Deep Sea Res. Oceanogr. Abstr.*, *20*(2), 111–140, doi:10.1016/0011-7471(73)90048-X.

Goyet, C., and A. Poisson (1989), New determination of carbonic acid dissociation constants in seawater as a function of temperature and salinity, *Deep Sea Res., Part A*, *36*(11), 1635–1654, doi:10.1016/0198-0149(89)90064-2.

Hansson, I. (1973), A new set of acidity constants for carbonic acid and boric acid in sea water, *Deep Sea Res., Oceanogr. Abstr.*, *20*(5), 461–478, doi:10.1016/0011-7471(73)90100-9.

Hauri, C., S. C. Doney, T. Takahashi, M. Erickson, G. Jiang, and H. W. Ducklow (2015), Two decades of inorganic carbon dynamics along the Western Antarctic Peninsula, *Biogeosciences*, *12*(9), 6929–6969, doi:10.5194/bgd-12-6929-2015.

Heywood, K. J., M. D. Sparrow, J. Brown, and R. R. Dickson (1999), Frontal structure and Antarctic bottom water flow through the Princess Elizabeth Trough, Antarctica, *Deep Sea Res., Part I*, *46*(7), 1181–1200, doi:10.1016/S0967-0637(98)00108-3.

Hobbs, W. R., R. Massom, S. Stammerjohn, P. Reid, G. Williams, and W. Meier (2016), A review of recent changes in Southern Ocean sea ice, their drivers and forcings, *Global Planet. Change*, *143*, pp. 228–250, doi:10.1016/j.gloplacha.2016.06.008.

Howard, S. L., J. Hyatt, and L. Padman (2004), Mixing in the pycnocline over the western Antarctic Peninsula shelf during Southern Ocean GLOBEC, *Deep Sea Res., Part II*, *51*(17–19), 1965–1979, doi:10.1016/j.dsr2.2004.08.002.

Ishii, M., H. Y. Inoue, H. Matsueda, and E. Tanoue (1998), Close coupling between seasonal biological production and dynamics of dissolved inorganic carbon in the Indian Ocean sector and the western Pacific Ocean sector of the Antarctic Ocean, *Deep Sea Res., I*, *45*, 1187–1209, doi:10.1016/S0967-0637(98)00010-7.

Jarvis, T., N. Kelly, S. Kawaguchi, E. van Wijk, and S. Nicol (2010), Acoustic characterisation of the broad-scale distribution and abundance of Antarctic krill (Euphausia superba) off East Antarctica (30-80°E) in January-March 2006, *Deep Sea Res., Part II*, *57*(9–10), 916–933, doi:10.1016/j.dsr2.2008.06.013.

Jennings, J. C., L. I. Gordon, and D. M. Nelson (1984), Nutrient depletion indicates high primary productivity in the Weddell Sea, *Nature*, *309*(5963), 51–54, doi:10.1038/309051a0.

Johnson, G. C. (2008), Quantifying Antarctic bottom water and north Atlantic Deep water volumes, *J. Geophys. Res.*, *113*, C05027, doi:10.1029/2007JC004477.

Jones, E. M., D. C. E. Bakker, H. J. Venables, and N. J. Hardman-Mountford (2015), Seasonal cycle of CO2 from the sea ice edge to island blooms in the Scotia Sea, Southern Ocean, *Mar. Chem.*, *177*, 490–500, doi:10.1016/j.marchem.2015.06.031.

Kaiser, J., M. K. Reuer, B. Barnett, and M. L. Bender (2005), Marine productivity estimates from continuous O_2/Ar ratio measurements by membrane inlet mass spectrometry, *Geophys. Res. Lett.*, *32*, L19605, doi:10.1029/2005GL023459.

Kara, A. B., P. A. Rochford, and H. E. Hurlburt (2003), Mixed layer depth variability over the global ocean, *J. Geophys. Res.*, *108*(C3), 3079, doi:10.1029/2000JC000736.

Kawaguchi, S., S. Nicol, P. Virtue, S. R. Davenport, R. Casper, K. M. Swadling, and G. W. Hosie (2010), Krill demography and large-scale distribution in the Western Indian Ocean sector of the Southern Ocean (CCAMLR Division 58.4.2) in Austral summer of 2006, *Deep Sea Res., Part II*, *57*(9–10), 934–947, doi:10.1016/j.dsr2.2008.06.014.

Khatiwala, S., F. Primeau, and T. Hall (2009), Reconstruction of the history of anthropogenic CO_2 concentrations in the ocean., *Nature*, *462*(7271), 346–349, doi:10.1038/nature08526.

Körtzinger, A. et al. (2000), The international at-sea intercomparison of fCO_2 systems during the R/V Meteor Cruise 36/1 in the North Atlantic Ocean, *Mar. Chem.*, *72*(2–4), 171–192, doi:10.1016/S0304-4203(00)00080-3.

Landschützer, P., et al. (2015), The reinvigoration of the Southern Ocean carbon sink., *Science*, *349*(6253), 1221–1224, doi:10.1126/science.aab2620.

Lannuzel, D., P. C. van der Merwe, A. T. Townsend, and A. R. Bowie (2014), Size fractionation of iron, manganese and aluminium in Antarctic fast ice reveals a lithogenic origin and low iron solubility, *Mar. Chem.*, *161*, 47–56, doi:10.1016/j.marchem.2014.02.006.

Laws, E. A. (1991), Photosynthetic quotients, new production and net community production in the open ocean, *Deep Sea Res., Part A*, *38*(1), 143–167, doi:10.1016/0198-0149(91)90059-O.

Le Corre, P., and H. J. Minas (1983), Distribution et évolution des éléments nutritifs dans le secteur indien de l'Océan Antarctique en fin de période estivale, *Oceanol. Acta*, *6*(4), 365–381.

Le Quéré, C. et al. (2007), Saturation of the southern ocean CO_2 sink due to recent climate change., *Science*, *316*(5832), 1735–1738, doi:10.1126/science.1136188.

Legge, O. J., D. C. E. Bakker, M. T. Johnson, M. P. Meredith, H. J. Venables, P. J. Brown, and G. A. Lee (2015), The seasonal cycle of ocean-atmosphere CO_2 flux in Ryder Bay, West Antarctic Peninsula, *Geophys. Res. Lett.*, *42*, 2934–2942, doi:10.1002/2015GL063796.

Lenton, A., F. Codron, L. Bopp, N. Metzl, P. Cadule, A. Tagliabue, and J. Le Sommer (2009), Stratospheric ozone depletion reduces ocean carbon uptake and enhances ocean acidification, *Geophys. Res. Lett.*, *36*, L12606, doi:10.1029/2009GL038227.

Lenton, A., et al. (2013), Sea–air CO_2 fluxes in the Southern Ocean for the period 1990–2009, *Biogeosciences*, *10*(6), 4037–4054, doi:10.5194/bg-10-4037-2013.

Li, X., D. M. Holland, E. P. Gerber, and C. Yoo (2014), Impacts of the north and tropical Atlantic Ocean on the Antarctic Peninsula and sea ice., *Nature*, *505*(7484), 538–542, doi:10.1038/nature12945.

Loose, B., W. R. McGillis, P. Schlosser, D. Perovich, and T. Takahashi (2009), Effects of freezing, growth, and ice cover on gas transport processes in laboratory seawater experiments, *Geophys. Res. Lett.*, *36*, L05603, doi:10.1029/2008GL036318.

Lueker, T. J., A. G. Dickson, and C. D. Keeling (2000), Ocean pCO_2 calculated from dissolved inorganic carbon, alkalinity, and equations for K1 and K2: Validation based on laboratory measurements of CO_2 in gas and seawater at equilibrium, *Mar. Chem.*, *70*(1–3), 105–119, doi:10.1016/S0304-4203(00)00022-0.

Marshall, J., and K. Speer (2012), Closure of the meridional overturning circulation through Southern Ocean upwelling, *Nat. Geosci.*, *5*(3), 171–180, doi:10.1038/ngeo1391.

Massom, R., P. Reid, S. Stammerjohn, B. Raymond, A. Fraser, and S. Ushio (2013), Change and variability in East antarctic sea ice seasonality, 1979/80-2009/10., *PLoS One*, *8*(5), e64756, doi:10.1371/journal.pone.0064756.

Mehrbach, C., C. H. Culberson, J. E. Hawley, and R. M. Pytkowicz (1973), Measurement of the apparent dissociation constants of carbonic acid in seawater at atmospheric pressure, *Limnol. Oceanogr.*, *18*(6), 897–907, doi:10.4319/lo.1973.18.6.0897.

Meijers, A. J. S. (2014), The Southern Ocean in the coupled model intercomparison Project phase 5., *Philos. Trans. R. Soc. A*, *372*(2019), 20130296, doi:10.1098/rsta.2013.0296.

Meijers, A. J. S., A. Klocker, N. L. Bindoff, G. D. Williams, and S. J. Marsland (2010), The circulation and water masses of the Antarctic shelf and continental slope between 30 and 80°E, *Deep Sea Res., Part II*, *57*(9–10), 723–737, doi:10.1016/j.dsr2.2009.04.019.

Miller, L. A., T. N. Papakyriakou, R. E. Collins, J. W. Deming, J. K. Ehn, R. W. Macdonald, A. Mucci, O. Owens, M. Raudsepp, and N. Sutherland (2011), Carbon dynamics in sea ice: A winter flux time series, *J. Geophys. Res.*, *116*, C02028, doi:10.1029/2009JC006058.

Millero, F. J. (2010), Carbonate constants for estuarine waters, *Mar. Freshwater Res.*, *61*(2), 139–142, doi:10.1071/MF09254.

Millero, F. J., D. Pierrot, K. Lee, R. H. Wanninkhof, R. Feely, C. L. Sabine, R. M. Key, and T. Takahashi (2002), Dissociation constants for carbonic acid determined from field measurements, *Deep Sea Res., Part I*, *49*(10), 1705–1723, doi:10.1016/S0967-0637(02)00093-6.

Millero, F. J., T. B. Graham, F. Huang, H. Bustos-Serrano, and D. Pierrot (2006), Dissociation constants of carbonic acid in seawater as a function of salinity and temperature, *Mar. Chem.*, *100*(1–2), 80–94, doi:10.1016/j.marchem.2005.12.001.

Mojica Prieto, F. J., and F. J. Millero (2002), The values of pK1 + pK2 for the dissociation of carbonic acid in seawater, *Geochim. Cosmochim. Acta*, *66*(14), 2529–2540, doi:10.1016/S0016-7037(02)00855-4.

Mucci, A. (1983), The solubility of calcite and aragonite in seawater at various salinities, temperatures, and one atmosphere total pressure, *Am. J. Sci.*, *283*(7), 780–799, doi:10.2475/ajs.283.7.780.

Nomura, D., M. A. Granskog, P. Assmy, D. Simizu, and G. Hashida (2013), Arctic and Antarctic sea ice acts as a sink for atmospheric CO_2 during periods of snowmelt and surface flooding, *J. Geophys. Res. Oceans*, *118*, 6511–6524, doi:10.1002/2013JC009048.

Nomura, D., H. Yoshikawa-Inoue, S. Kobayashi, S. Nakaoka, K. Nakata, and G. Hashida (2014), Winter to summer evolution of pCO_2 in surface water and air–sea CO_2 flux in the seasonal ice zone of the Southern Ocean, *Biogeosciences*, *11*, 5749–5761, doi:10.5194/bgd-11-657-2014.

Ohshima, K. I., et al. (2013), Antarctic bottom water production by intense sea-ice formation in the Cape Darnley polynya, *Nat. Geosci.*, *6*(3), 235–240, doi:10.1038/ngeo1738.

Orsi, A. H., T. Whitworth, and W. D. Nowlin (1995), On the meridional extent and fronts of the Antarctic Circumpolar Current, *Deep Sea Res., Part I*, *42*(5), 641–673, doi:10.1016/0967-0637(95)00021-W.

Orsi, A. H., G. C. Johnson, and J. L. Bullister (1999), Circulation, mixing, and production of Antarctic Bottom Water, *Prog. Oceanogr.*, *43*(1), 55–109, doi:10.1016/S0079-6611(99)00004-X.

Pardo, P. C., F. F. Pérez, S. Khatiwala, and A. F. Ríos (2014), Anthropogenic CO_2 estimates in the Southern Ocean: Storage partitioning in the different water masses, *Prog. Oceanogr.*, *120*, 230–242, doi:10.1016/j.pocean.2013.09.005.

Park, Y.-H., E. Charriaud, and M. Fieux (1998), Thermohaline structure of the Antarctic Surface Water/Winter Water in the Indian sector of the Southern Ocean, *J. Mar. Syst.*, *17*(1–4), 5–23, doi:10.1016/S0924-7963(98)00026-8.

Pasquer, B., M. Mongin, N. Johnston, and S. Wright (2010), Distribution of particulate organic matter (POM) in the Southern Ocean during BROKE-West (30°E - 80°E), *Deep Sea Res., Part II*, *57*(9–10), 779–793, doi:10.1016/j.dsr2.2008.12.040.

Peng, T.-H., T. Takahashi, W. S. Broecker, and J. Olafsson (1987), Seasonal variability of carbon dioxide, nutrients and oxygen in the northern North Atlantic surface water: Observations and a model, *Tellus Ser. B*, *39B*(5), 439–458, doi:10.1111/j.1600-0889.1987.tb00205.x.

Pierrot, D., C. Neill, K. Sullivan, R. Castle, R. H. Wanninkhof, H. Lüger, T. Johannessen, A. Olsen, R. A. Feely, and C. E. Cosca (2009), Recommendations for autonomous underway pCO_2 measuring systems and data-reduction routines, *Deep Sea Res., Part II*, *56*(8–10), 512–522, doi:10.1016/j.dsr2.2008.12.005.

Redfield, A. C., B. H. Ketchum, and F. A. Richards (1963), The influence of organisms on the composition of seawater, in *The Sea*, vol.2, edited by M. N. Hill, pp. 26–79, Wiley-Interscience, New York.

Reuer, M. K., B. A. Barnett, M. L. Bender, P. G. Falkowski, and M. B. Hendricks (2007), New estimates of Southern Ocean biological production rates from O_2/Ar ratios and the triple isotope composition of O_2, *Deep Sea Res., Part I*, *54*(6), 951–974, doi:10.1016/j.dsr.2007.02.007.

Revelle, R., and H. E. Suess (1957), Carbon dioxide exchange between atmosphere and ocean and the question of an increase of atmospheric CO_2 during the past decades, *Tellus*, *9*(1), 18–27, doi:10.1111/j.2153-3490.1957.tb01849.x.

Roden, N. P., E. H. Shadwick, B. Tilbrook, and T. W. Trull (2013), Annual cycle of carbonate chemistry and decadal change in coastal Prydz Bay, East Antarctica, *Mar. Chem.*, *155*, 135–147, doi:10.1016/j.marchem.2013.06.006.

Rosenberg, M., and R. Gorton (2006), BROKE-West Survey, Marine Science Cruise AU603: Oceanographic Field Measurements and Analysis, technical report, Australian Antarctic Data Centre in Hobart, Tasmania, Australia, doi:10.4225/15/58058ce3994de, [Available at http://data.aad.gov.au/aadc/metadata/metadata_redirect.cfm?md=/AMD/AU/BROKE-West_CTD_au0603.]

Roy, R. N., L. N. Roy, K. M. Vogel, C. Porter-Moore, T. Pearson, C. E. Good, F. J. Millero, and D. M. Campbell (1993), The dissociation constants of carbonic acid in seawater at salinities 5 to 45 and temperatures 0 to 45°C, *Mar. Chem.*, *44*(2–4), 249–267, doi:10.1016/0304-4203(93)90207-5.

Rubin, S. I., T. Takahashi, D. W. Chipman, and J. G. Goddard (1998), Primary productivity and nutrient utilization ratios in the Pacific sector of the Southern Ocean based on seasonal changes in seawater chemistry - A comparative study, *Deep Sea Res., Part I*, *45*(8), 24, doi:10.1016/S0967-0637(98)00021-1.

Sabine, C. L., et al. (2004), The oceanic sink for anthropogenic CO_2, *Science*, *305*(5682), 367–371, doi:10.1126/science.1097403.

Schallenberg, C., P. van der Merwe, F. Chever, J. T. Cullen, D. Lannuzel, and A. R. Bowie (2015), Dissolved iron and iron(II) distributions beneath the pack ice in the East Antarctic (120°E) during the winter/spring transition, *Deep Sea Res., Part II*, *131*, 96–110, doi:10.1016/j.dsr2.2015.02.019.

Schwarz, J. N., B. Raymond, G. D. Williams, B. Pasquer, S. J. Marsland, and R. J. Gorton (2010), Biophysical coupling in remotely-sensed wind stress, sea surface temperature, sea ice and chlorophyll concentrations in the South Indian Ocean, *Deep Sea Res., Part II 57*(9–10), 701–722, doi:10.1016/j.dsr2.2009.06.014.

Sedwick, P. N., and G. R. DiTullio (1997), Regulation of algal blooms in Antarctic Shelf Waters by the release of iron from melting sea ice, *Geophys. Res. Lett.*, *24*(20), 2515–2518, doi:10.1029/97GL02596.

Semiletov, I., A. Makshtas, and S. I. Akasofu (2004), Atmospheric CO_2 balance: The role of Arctic sea ice, *Geophys. Res. Lett.*, *31*, L05121, doi:10.1029/2003GL017996.

Shadwick, E. H., B. Tilbrook, and G. D. Williams (2014), Carbonate chemistry in the Mertz Polynya (East Antarctica): Biological and physical modification of dense water outflows and the export of anthropogenic CO_2, *J. Geophys. Res. Oceans*, *119*, 1–14, doi:10.1002/2013JC009286.

Smith, W. O., and D. M. Nelson (1986), Importance of ice edge phytoplankton production in the Southern Ocean, *Bioscience*, *36*, 251–257, doi:10.2307/1310215.

Sokolov, S., and S. R. Rintoul (2007), On the relationship between fronts of the Antarctic Circumpolar Current and surface chlorophyll concentrations in the Southern Ocean, *J. Geophys. Res.*, *112*, C07030, doi:10.1029/2006JC004072.

Stammerjohn, S. E., D. G. Martinson, R. C. Smith, X. Yuan, and D. Rind (2008), Trends in Antarctic annual sea ice retreat and advance and their relation to El Niño-Southern Oscillation and Southern Annular Mode variability, *J. Geophys. Res. Oceans*, *113*, C03S90, doi:10.1029/2007JC004269.

Sweeney, C., D. A. Hansell, C. A. Carlson, L. A. Codispoti, L. I. Gordon, J. Marra, F. J. Millero, W. O. Smith, and T. Takahashi (2000), Biogeochemical regimes, net community production and carbon export in the Ross Sea, Antarctica, *Deep Sea Res., Part II*, *47*(15–16), 3369–3394, doi:10.1016/S0967-0645(00)00072-2.

Takahashi, T., C. Sweeney, B. Hales, D. Chipman, T. Newberger, J. Goddard, R. Iannuzzi, and S. Sutherland (2012), The changing carbon cycle in the Southern Ocean, *Oceanography*, *25*(3), 26–37, doi:10.5670/oceanog.2012.71.

Thompson, D. W. J., S. Solomon, P. J. Kushner, M. H. England, K. M. Grise, and D. J. Karoly (2011), Signatures of the Antarctic ozone hole in Southern Hemisphere surface climate change, *Nat. Geosci.*, *4*(11), 741–749, doi:10.1038/ngeo1296.

Touratier, F., and C. Goyet (2004), Definition, properties, and Atlantic Ocean distribution of the new tracer TrOCA, *J. Mar. Syst.*, *46*(1–4), 169–179, doi:10.1016/j.jmarsys.2003.11.016.

Touratier, F., L. Azouzi, and C. Goyet (2007), CFC-11, $\Delta^{14}C$ and ^3H tracers as a means to assess anthropogenic CO_2 concentrations in the ocean, *Tellus B*, *59*(2), 318–325, doi:10.1111/j.1600-0889.2006.00247.x.

van Heuven, S., D. Pierrot, J. W. B. Rae, E. Lewis, and D. W. R. Wallace (2011), MATLAB Program developed for CO_2 system calculations, *ORNL/CDIAC-105*, Carbon Dioxide Inf. Anal. Center, Oak Ridge Natl. Lab. U.S. Dep. Energy, Oak Ridge, Tennessee, US, doi:10.3334/CDIAC/otg.CO2SYS_MATLAB_v1.1.

van Heuven, S. M. A., M. Hoppema, E. M. Jones, and H. J. W. de Baar (2014), Rapid invasion of anthropogenic CO_2 into the deep circulation of the Weddell Gyre, *Philos. Trans. R. Soc. A*, *372*(2019), 20130056, doi:10.1098/rsta.2013.0056.

Venables, H. J., A. Clarke, and M. P. Meredith (2013), Wintertime controls on summer stratification and productivity at the western Antarctic Peninsula, *Limnol. Oceanogr.*, *58*(3), 1035–1047, doi:10.4319/lo.2013.58.3.1035.

Virtue, P. et al. (2010), Krill growth and condition in Western Indian Ocean sector of the Southern Ocean 30-80°E in austral summer 2006, *Deep Sea Res., Part II*, *57*(9–10), 948–955, doi:10.1016/j.dsr2.2008.11.035.

Wanninkhof, R. (2014), Relationship between wind speed and gas exchange over the ocean revisited, *Limnol. Oceanogr. Methods*, *12*(6), 351–362, doi:10.4319/lom.2014.12.351.

Wanninkhof, R. H., et al. (2013), Global ocean carbon uptake: Magnitude, variability and trends, *Biogeosciences*, *10*(3), 1983–2000, doi:10.5194/bg-10-1983-2013.

Weiss, R. F. (1974), Carbon dioxide in water and seawater: The solubility of a non-ideal gas, *Mar. Chem.*, *2*(3), 203–215, doi:10.1016/0304-4203(74)90015-2.

Westwood, K. J., B. F. Griffiths, K. M. Meiners, and G. D. Williams (2010), Primary productivity off the Antarctic coast from 30°–80°E; BROKE-West survey, 2006, *Deep Sea Res., Part II*, *57*(9–10), 794–814, doi:10.1016/j.dsr2.2008.08.020.

Whitworth, T., A. H. Orsi, S.-J. Kim, W. D. Nowlin, and R. A. Locarnini (1998), *Ocean, Ice, and Atmosphere: Interactions at the Antarctic Continental Margin, Antarct. Res. Ser.*, vol. 3, edited by S. S. Jacobs and R. F. Weiss, AGU, Washington, D. C.

Williams, G. D., S. Nicol, S. Aoki, A. J. S. Meijers, N. L. Bindoff, Y. Iijima, S. J. Marsland, and A. Klocker (2010), Surface oceanography of BROKE-West, along the Antarctic margin of the south-west Indian Ocean (30-80°E), *Deep Sea Res., Part II*, *57*(9–10), 738–757, doi:10.1016/j.dsr2.2009.04.020.

Williams, G. D., et al. (2016), The suppression of Antarctic bottom water formation by melting ice shelves in Prydz Bay, *Nat. Commun.*, *7*, 12577, doi:10.1038/ncomms12577.

Wright, S. W., R. L. van den Enden, I. Pearce, A. T. Davidson, F. J. Scott, and K. J. Westwood (2010), Phytoplankton community structure and stocks in the Southern Ocean (30–80°E) determined by CHEMTAX analysis of HPLC pigment signatures, *Deep Sea Res., Part II*, *57*(9–10), 758–778, doi:10.1016/j.dsr2.2009.06.015.

Yager, P. L., D. W. R. Wallace, K. M. Johnson, W. O. Smith, P. J. Minnett, and J. W. Deming (1995), The Northeast Water Polynya as an atmospheric CO_2 sink: A seasonal rectification hypothesis, *J. Geophys. Res.*, *100*(C3), 4389–4398, doi:10.1029/94JC01962.

Zemmelink, H. J., B. Delille, J. L. Tison, E. J. Hintsa, L. Houghton, and J. W. H. Dacey (2006), CO_2 deposition over the multi-year ice of the western Weddell Sea, *Geophys. Res. Lett.*, *33*, L13606, doi:10.1029/2006GL026320.